EVALUATION OF A HIGH PRESSURE PROPORTIONAL COUNTER FOR THE DETECTION OF RADIOACTIVE NOBLE GASES

THESIS

Richard E. Lackey
Major, U.S. Army

DEPARTMENT OF THE AIR FORCE
AIR UNIVERSITY
AIR FORCE INSTITUTE OF TECHNOLOGY

Wright-Patterson Air Force Base, Ohio

AFIT/GNE/PH/84M-9

EVALUATION OF A HIGH PRESSURE PROPORTIONAL COUNTER FOR THE DETECTION OF RADIOACTIVE NOBLE GASES

THESIS

Richard E. Lackey
Major, U.S. Army

Approved for public release; distribution unlimited

AFIT/GNE/PH/84M-9

EVALUATION OF A HIGH PRESSURE PROPORTIONAL COUNTER FOR THE DETECTION OF RADIOACTIVE NOBLE GASES

THESIS

Presented to the Faculty of the School of Engineering

of the Air Force Institute of Technology

Air University

In Partial Fulfillment of the

Requirements for the Degree of

Master of Science in Nuclear Engineering

Richard E. Lackey, B.S.Ch.E

Lieutenant Colonel

January 1987

Preface

This thesis summarizes more than ten months of study, research and analysis of a new detector system. It culminates a determined effort to resurrect eighteen-year old physics skills.

For instilling the will to persevere and achieve this long held goal, I wish to acknowledge my parents' efforts. I want also to publicly express my deep gratitude to my wife Carolyn for her support, and to my children Carla Anne and Brian for their patience in doing without a dad during this time. I would further acknowledge that while providing the moral support in my efforts, my wife gracefully completed her own graduate studies, Summa Cum Laude.

Finally, I offer my most profound thanks to Dr. George John for his guidance, help and patience. His selfless efforts were critical in the ultimate successful completion of these academic endeavors.

R.E. Lackey
Major, U.S. Army

Table of Contents

List of Figures

List of Tables

Abstract

This report presents a study of the characteristics of a high pressure proportional detector for the qualitative and quantitative analysis of radioactive noble gases. Several external sources (^{241}Am, ^{109}Cd & ^{57}Co) were used to establish the detector's response at high pressures (~~20 and 50 atmospheres~~) using argon fill gas. A radioactive xenon gas sample with ^{131m}Xe and ^{133}Xe was used to demonstrate the detector's utility for the analysis of radioactive noble gases.

Procedurally, counting gas from a 12.34-liter reservoir was cryogenically condensed in the 0.197-liter detector volume. The gas was purified through repeated passes across zirconium-titanium turnings at 1000°C, using a manual cryogenic pumping process. The cylindrical stainless steel detector is nominally 5.25 inches in length with a 1.625-inch inner diameter and a 0.0003-inch stainless steel anode wire.

Energy calibration was performed using the external sources. Intrinsic efficiency for the detector was initially high (to 95%) with energy resolution to 12% fwhm for ^{57}Co photopeaks (~122 keV) using argon fill gas at fifty atmospheres. Subsequent effects of a contaminant inadvertently introduced into the detector could not be fully eliminated. Though improved gas purification techniques produced resolutions to 9% fwhm, intrinsic efficiencies varied, and were reduced to 3.2% (^{57}Co ~122 keV photopeak).

The analysis of the internal radioactive xenon gas source was not successful. The ^{131m}Xe to ^{133}Xe concentration was 50% of the planned minimum value, and the ^{133}Xe source activity was one hundred times the

cont'd

acceptable level. The associated detector recovery time and space charge density reduced the efficiency drastically (~1%). Occasional unpredictable responses from contaminants adsorbed in the epoxy seals produced excessive numbers of erratic data with the internal noble gas source.

Contaminated end cap materials should be replaced before continuing work with this system. The principal limitation to the current system is the manually performed purification process. Specific designs are detailed to provide for a continuous counting gas purification system. Further research using this detection system is suggested.

EVALUATION OF A HIGH PRESSURE PROPORTIONAL COUNTER FOR THE DETECTION OF RADIOACTIVE NOBLE GASES

I. INTRODUCTION

General

This thesis presents an evaluation of a detection system for analyzing low activities and concentrations of radioactive noble gases. Several important sources of noble gas radionuclides require quantitative and qualitative analysis. Local feasibility studies have been conducted with detection systems based upon several of the most appropriate and promising detectors identified from the literature. The purpose of this study was to evaluate the detection system based on a high pressure proportional counter which was designed, assembled and initially tested by J. Knapp in 1983 (34). As with previous local studies, this investigation focused on radioactive samples of one noble gas, xenon. The general approach was to characterize the detector using external gamma sources and purified argon fill gas at pressures of twenty and fifty atmospheres. A sample of ^{131m}Xe and ^{133}Xe was then used to test the system.

The remainder of this chapter elaborates on some of the more significant background considerations, provides a more precise definition of the purpose and scope of this study, describes in more detail the general approach taken in the research, and finally, outlines the remainder of this report.

Background

Radioactive noble gases which are otherwise in low abundance in the atmosphere are associated with releases from nuclear reactors, nuclear fuel reprocessing plants, detonations of nuclear devices, and, to a lesser extent, by naturally occurring processes and phenomena. Qualitative and quantitative analysis of low activities and concentrations of radioactive noble gases from atmospheric samples are required by the Nuclear Regulatory Commission in conjunction with licensing and monitoring procedures for nuclear facilities. Additionally, the Non-Proliferation Treaty of 1970 and numerous other bilateral treaties provide for world-wide monitoring of releases of radioactive materials including radioactive noble gases. Krypton and xenon isotopes are of particular interest.

Research Described in the Literature. Several devices already have performed, or theoretically could perform, this analysis. Four primary systems are considered which have resulted in local feasibility studies. The most widely used system is based upon the liquid scintillation counter. Horrocks and Studier used this detection system for their radioactive noble gas research in 1964. They reported intrinsic efficiencies which approached one hundred percent for electrons, but were substantially less for electromagnetic radiation. The latter results were due to low absorption coefficients of the scintillation media. Additionally, this detector suffered from poor spectral resolution (28:2078). As one of the first detection systems to be successfully used in the study of noble gas radionuclides, these results are cited as a basis for comparison when evaluating other detection systems.

A second approach described in the literature is based on the

liquid ionization chamber using liquefied noble gas for the detection media. This system enjoys high intrinsic efficiencies because gas samples are mixed with the detection media as is the case with liquid scintillation detectors. Also, higher absorption coefficients associated with liquefied noble gases result in better efficiencies for detecting photons. Most importantly, the noble gas ionization chamber has significantly better resolution as reported in 1975 by Shibamura et al. in related research (50:255).

A third system for detecting radioactive noble gases is based on semiconductor detectors. These detectors have inherently good resolution, but must overcome problems associated with low absolute efficiencies since the source is outside the sensitive volume of the detector. Additional effects which must be minimized include self-absorption in other than small samples and absorption by the sample container.

The final system considered is based on the proportional counter which is often used in the detection and spectroscopy of low energy photons. Its resolution and intrinsic efficiency are greater than liquid scintillation detectors for electromagnetic radiation. Further, problems with self-absorption and geometry are eliminated because gas samples are mixed with the detector's sensitive media as with liquid scintillation and liquid ionization chamber detectors. High pressures have been utilized in proportional counters to improve confinement of charged particles and to increase absorption of photons within the detector's sensitive volume. Several studies have been conducted to determine the utility of this approach. In Schell's 1968 study of internal gas proportional counters for measuring low-level environmental radionuclides, resolutions to 27% fwhm and intrinsic efficiencies to

75% were reported when counting ^{37}Ar (2.6 keV x-rays and Auger electrons) at pressures to ten atmospheres (49). In 1973 Baerg (2), and Legrand et al. (39), separately reported measurements of internal conversion electrons (33-166 keV) in high pressure proportional counters with 4π geometry at pressures to seventy atmospheres. Resolutions of 18-25% fwhm and intrinsic efficiencies to 100% were cited. Other related research using high pressure proportional counters includes reports of 22-27% fwhm resolutions for pressures from 10 to 40 atmospheres with ^{55}Fe 5.9 keV photons by Bamberger (3); a report of 2.7% resolution for the 60 keV full energy peak of ^{241}Am by Batchelor et al. (5); studies to 4 atmospheres by Costa et al. (16); and studies to 100 atmospheres by Gilmer (23).

Local Feasibility Studies. These detector systems were utilized for local feasibility studies. Various schemes were developed to optimize each detection systems' resolution and efficiency to specifically analyze radioactive noble gases. Test samples of ^{131m}Xe and ^{133}Xe were used for evaluations. Systems based on the semiconductor detector, the liquid ionization chamber and the high pressure proportional counter have been investigated.

In 1974 Rowe (48) designed and constructed a detection system based on the SiLi detector. Findings of that study suggested that the lack of reproducible data resulted from the cryogenic methodology used in condensing the sample. Other analysis showed these fluctuations to be within tolerances associated with the counting statistics (32:26,27). Modifications to the sample chamber were made in 1976 by Hunt (29), which allowed the gas sample to be evenly deposited. Findings in this study listed problems in quantifying x-ray fluorescence in the carrier

gas, degradation of electron energies from self-absorption and difficulties related to geometry considerations. Further modifications were made in 1982 by Andrews (1) to minimize these problems. This system was successfully used to measure the activity of ^{131m}Xe in the presence of ^{133}Xe using a three step procedure. Typical resolutions and efficiencies reported include 7% and 0.6% for internal conversion electrons (129-158 keV), 1% and 0.5% for gamma radiation photopeaks (81 keV), and, 22% and 5.2% for x-rays (30 keV).

Concurrently, a study based on the liquefied noble gas ionization chamber was initiated by Berggren in 1982 (8). This approach offered the opportunity of achieving efficiencies comparable to liquid scintillation detectors and resolutions approaching those of semiconductor detectors. This combination would make the liquid ionization chamber detection system superior to both of those based on the scintillation or semiconductor detector systems for xenon analysis. Berggren's data indicated problems with corona discharge and position dependent fluctuations. This effort was continued in 1983 by Benedetti (6), who installed a new parallel plate sample chamber to eliminate the discharges and a Frisch grid to remove the position dependence. The results were not conclusive. Gibbons (21) in 1984 continued this research with additional modifications to the detector. Energy resolutions of 45% were typical with intrinsic efficiencies to 70% (^{241}Am 60 keV photons). Electronegative impurities in the liquefied carrier gas and discharges in the vapor phase noble gas above the chamber were suggested as the main problems with the detector. Differentiation of the ^{131m}Xe and ^{133}Xe radioisotopes could not be accomplished.

A third research effort focused upon a detection system based on the high pressure proportional counter. This system was designed, assembled and initially tested by Knapp (34) in 1983. Principle reasons for investigating the use of a high pressure proportional counter were the theoretically superior resolutions and the high intrinsic efficiencies compared to those of liquid scintillation detectors. Using 160 keV gamma radiation as a basis for comparison, Knapp calculated the theoretical limits for the resolutions of various detectors. Semiconductor detectors offered the best resolutions as expected. However, the predicted resolution for atmospheric proportional counters was seven times better than for liquid scintillation counters and nearly equalled that of liquid ionization chambers (34:6) Further details are developed in Chapter II. Additionally, since higher pressures improve confinement of charged particles and increase absorption of photons within the detector's sensitive volume, this would suggest even better signals and resolutions at higher pressures. For example, xenon fill gas at fifty atmospheres reduces the atmospheric range of 160 keV electrons from 10.75 cm to 0.21 cm. This would also result in higher intrinsic efficiencies.

Implementing this approach, Knapp's first detector design was similar to Batchelor's cylindrical counter with screw-in end plates and axially positioned anode wire. This detector suffered from poor alignment and developed excessive leaks. A second detector, similarly designed, utilized flange-type end plates bolted into the cylindrical counter body and used soft copper gasket rings. The stainless steel detector was 5.25 inches in length with a 3.0 inch outer diameter and a 1.625 inch inner diameter. It had a 0.5 mil stainless steel anode

wire. Findings of this study listed problems with electrical discharges from external connections at high voltages which precluded evaluation at full operating voltages. Also, response characteristics of the second detector deteriorated with time. This problem was described as energy spectra breaking out into several small peaks accompanied by a large loss in overall gain. Conclusions suggested this problem was a result of impurities from outgassing. Leaks were specifically described as not measurable or significant. Spectra from external sources used with unpurified technical grade P-10 gas (90% Ar - 10% CH_4) at pressures of one and fifty atmospheres demonstrated that the detector was functional, but could not adequately characterize the detector's response. Due to the thickness of the stainless steel cathode wall (0.69 inches), sources available for calibration were either excessively energetic or not energetic enough to be fully measured. The high pressure spectra was not conclusive. Finally, the results and spectra from the test sample of ^{133}Xe was also not conclusive as a result of equipment failure during the run. Though not fully characterized, a functional proportional detection system was available for further study and research as a result of this effort.

Purpose and Scope

The purpose of this investigation is to continue the study of this high pressure proportional counter. Specifically, the detector's operating characteristics and resolutions at various high pressures are to be evaluated. As with the other local research discussed, the main goal is to determine the utility of this detection system to

qualitatively and quantitatively analyze low activities and concentrations of radioactive noble gases from atmospheric samples.

Argon is used as the principle detection media. External sources used to calibrate the detector included ^{241}Am, ^{109}Cd and ^{57}Co. The high pressures were limited to twenty and fifty atmospheres. A sample of ^{131m}Xe and ^{133}Xe was used to demonstrate the feasibility of the system to quantitatively and qualitatively differentiate these noble gas radioisotopes.

General Approach

The general approach taken in continuing this research was to initially modify the detector to minimize or eliminate the problems with internal or external electrical discharges. Secondly, a smaller diameter anode wire was installed which reduced the operating voltages required. The theoretical basis for this approach is developed in Chapter II. The final modification to the detector itself was the installation of several small diameter wells in the top of the detector's thick, stainless steel outer case. This reduced the wall thickness at the base of the wells from 0.69 inches to approximately 0.035 inches. This reduction allowed the selection of external gamma sources of moderate energies to be utilized to characterize the detector response. These sources and energies were comparable to the energies associated with the radioactive xenon test sample.

The basis for introducing samples into the detector and for quantifying fill gas pressures was to cryogenically condense known quantities of gases from the gas handling system into the detector's cold finger. Therefore, initial operation of the system was delayed

to allow accurate volumetric measurements to be made. The process was accomplished by allowing a known volume of gas to be expanded selectively into specific segments of the detector and gas handling system. Gas laws and accurate pressure measurements were used to calculate the necessary volumes.

Following these volumetric measurements, parametric studies of the detector were accomplished using external sources and atmospheric argon gas. Subsequently, techniques associated with the purification process were refined until stable high pressure data could be predictably obtained.

Data was then collected for a range of operating voltages at pressures of twenty and fifty atmospheres using argon gas and the external sources. These sources included ^{241}Am, ^{109}Cd and ^{57}Co with their respective 59.54 keV, 88.03 keV and 122.01 keV gamma radiations. Optimum operating conditions were noted which produced the best resolutions.

Finally, a single radioactive sample of xenon was introduced to demonstrate the utility of this detection system to quantitatively and qualitatively measure dilute amounts of ^{131m}Xe in ^{133}Xe.

Sequence of Report

The remainder of this report provides additional theoretical development and background information, detailed descriptions of equipment and procedures used, and, a detailed discussion of the results and conclusions of this study.

Specifically, Chapter II reviews the basic theory of the operation of high pressure proportional detectors. The principle processes

which produce the discharge or signal pulse are discussed sequentially. The concept of gas multiplication is a significant aspect of this development. Time characteristics of the signal, factors which influence the magnitude of the pulse, and, development of the statistical considerations associated with energy resolution are presented.

Following the development of the theory of the detector itself, Chapter III provides the necessary background regarding the decay schemes of the radioactive sources and the most pertinent physical characteristics of the argon detecting media. Chapter IV describes the detector, the gas handling system and the supporting equipment which comprise this detection system. The procedures used to purify the carrier gas, to introduce the internal samples, and to operate the detector and electronics are detailed in Chapter V. Overall results and representative data are presented in Chapter VI. Finally, conclusions and recommendations of this study are discussed in Chapter VII.

II. Theory

Introduction

The high pressure detection system uses the proportional counter to detect ionizing radiation. Its operation is based on collecting electrons and positive ions which result from radiation quanta ionizing the detection media. Charged particle radiation directly ionizes the fill gas as it is stopped within the sensitive volume of the detector. However, uncharged radiation quanta first interacts with the counting gas or detector wall to produce a charged particle within the detector's sensitive volume. This, in turn, produces ionization as in the first case.

The output signal pulse from the detector depends on the number of primary ion pairs (electrons and positive ions) formed. This number is directly proportional to the energy deposited from the radiation quanta and inversely proportional to the average energy required to produce an ion pair. The latter value, unique to each fill gas, is called the W-value.

The process of gas multiplication develops a significant number of secondary ion pairs and increases the signal, which would otherwise develop from primary ion pairs alone. Primary electrons drift to the anode with increasing speed, while more massive positive ions slowly accelerate toward the cathode. Within a few mean free paths from the anode, electrons gain sufficient kinetic energy between collisions with neutral fill gas atoms to produce additional ionization. This is the gas multiplication process, or so called Townsend avalanche.

The characteristic signal from this detector is developed by the collection of the total charge of the ion pairs formed. Electrons arrive at the anode in a few microseconds. However, positive ions, nearly two thousand times more massive, move more slowly, are collected on the order of a few milliseconds and principally determine the time characteristics of the signal pulse.

Several competing processes, including the build up of space charge and spurious pulses, reduce the quality of the output signal. Slowly moving positive ions may alter the electric field by self-induced or general space charge, reducing the gas multiplication proportionality for subsequent radiation quanta. This multiplication process produces an abundance of positive ions near the surface of the anode. If the multiplication factor is sufficiently high, a sheath of positive charge develops near the anode, significantly altering the electric field. Additionally, when the number of radiation quanta detected is sufficiently large, the electric field is modified by the high density of positive ions dispersed throughout the volume of the detector.

Spurious pulses also influence the quality of the signal. In addition to causing ionization, radiation quanta excite some of the fill gas atoms. Excited gas atoms may emit ultra-violet photons in returning to the ground state. These photons interact with the cathode wall of the detector, causing electrons to be emitted. Additionally, positive ions and neutral gas atoms colliding with the detector wall may produce similar emissions. These spurious pulses or after pulses alter the primary signal. Certain additive gas molecules or noble gas mixtures serve to quench or reduce these effects.

The resolution of the output signal pulse is affected by space

charge, spurious pulses and other competing processes. The ability of the detector to resolve fine details from spectra can be related to the effects which cause variations in the number of primary ion pairs, or to those effects which cause a variation in the multiplication factor. Certain design criteria can optimize the operating characteristics of the detector and improve energy resolution of the spectra.

This chapter discusses the theory involved in the interactions of radiation with the counting gas, the gas multiplication process and the characteristics of the ideal signal pulse. Also, competing processes that reduce the signal, limitations to the resolution of the signal, and design considerations which optimize the response of the detector are presented.

Detecting Radiation

Studies of radioactive material require the quantitative detection and measurement of the radiation emitted. Detecting the radiation quanta results from interactions in the counting gas which are different for charged or uncharged radiation. Theoretical relations have been developed which describe the ability of the detecting media to stop charged particles or to absorb photons. These correlations are related to the detector's efficiency.

Radioactivity. A discussion of radiation begins with Bohr's simple model of the atom where negatively charged electrons orbit a central nucleus of positively charged photons and uncharged neutrons. Atoms with excessively high (excited) energy states or atoms with an unstable number of protons, neutrons or electrons return to more stable forms by emitting radiation. These emissions may be electromagnetic

radiation (x-rays or gamma rays) or some combination of sub-atomic particles (electrons, protons, neutrons, etc.) which are expelled from the atom. The type of radiation, the rate at which the radiation is emitted, and the energy level of those radiations are unique to each radionuclide.

Interaction with Matter. This radiation interacts with matter differently depending on whether it is electrically charged or not. Charged particles impart enough localized energy to absorbing material to ionize atoms and molecules through coulombic interactions. Whereas, uncharged particles and electromagnetic radiation initially generate (via absorption or scatter reactions) energetic electrons which cause secondary ionization by their movement through the absorbing material, as in the first case. This characteristic ionization is the basis for most radiation detectors (33:40).

Detectors. Many detectors are based upon the process of separating and collecting the electrons and positive ions produced by the ionizing radiation. This collection process is accomplished through the presence of an electric field in the detector. The moving charges constitute a current which can be electronically measured. Alternately, the total charge collected per quantum of radiation can be recorded as a single output pulse. The latter mode of operation is most frequently employed.

Calculating Particles Emitted. The ability of a detector to record a count for each given type of radiation quantum entering the detector's sensitive volume is known as its intrinsic efficiency. A radionuclide with a given activity may emit several different types of radiation. Branching ratios specify their relative fraction per

emission. The number of particles emitted over a given counting time is given by

$$N_i = \frac{f_i S}{\lambda} (1 - e^{-\lambda t_c}) \qquad (2.1)$$

where

N_i = number of i-th quanta emitted

f_i = branching ratio of i-th quanta emitted, where the branching ratio is the fractional decay probability, usually expressed in percentages, of a transition from a given state to a lower state.

S = activity of the source

t_c = time of the count

λ = radionuclide decay constant

When the counting time is very short in comparison to the half-life of the radionuclide, a Taylor series expansion simplifies the previous relation to

$$N_i = f_i \cdot S \cdot t_c \qquad (2.2)$$

Efficiency of Counting. The efficiency of producing a full-energy peak for photons depends on several factors. These include: reduction of intensity by spherical divergence; losses caused by scatter and absorption reactions of all kinds by the material between the source and the detecting medium; and losses of radiation quanta which escape after reaching the detector media. The measured counts, C_{TH}, can be estimated as

$$C_{TH} = f_g \cdot f_t \cdot f_s \cdot N_i \qquad (2.3)$$

where

f_g = geometric factor which depends on source position, configuration (disc or point source) and area of entrance window to detector

f_t = fraction transmitted by absorbers which accounts for losses of radiation quanta scattered or absorbed by source, air, windows, or other intervening media.

f_s = factor to account for quanta absorbed or stopped within the sensitive volume of the detector while the balance is considered to have escaped.

Geometric Reduction Factor. Though the geometric factor for an internal source is one-hundred percent, isotropic radiation emitted from an external source is reduced in intensity by spherical divergence. This external geometric factor is given by

$$f_g = \Omega/4\pi \tag{2.4}$$

where

Ω = solid angle (in Steradians) subtended by the detector from the source position.

For a right cylindrical detector surface at a distance from an external point source, the geometric factor is given by (35:95)

$$f_g = (1 - d/(d^2 + r^2)^{0.5})/2 \tag{2.5}$$

where

d = distance of the detector aperture from the source

r = radius of the circular detector aperature

Transmission Factor for Intervening Materials. An external collimated beam of photons, using so called good geometry, may be absorbed or scattered from the beam by the material encountered between the source and the detector. It is assumed that scattered photons do not enter the detector (or are not detected under the full-energy peak), then the fraction of photons transmitted through the intervening material is given by

$$f_t = \exp (- (\mu/\rho)_t \rho\chi) \tag{2.6}$$

where

$(\mu/\rho)_t$ = total absorption coefficient for the intervening material

ρ = density of intervening material

χ = thickness of intervening material

In this research, due to the thickness of the detector's case and the lack of thin entrance windows, external sources of charged particles are stopped before reaching the detector's sensitive volume (resulting in $f_t = 0$). Therefore, external particulate sources are not considered further.

Reduction Factor for Photon Escape. A fraction of the photons which enter the detector from an external source, or those emitted from an internal source, are stopped within the sensitive volume of the detector. The principal interactions of interest are photoelectric absorption and Compton scattering. The remainder escape from the detector. Photoelectric interactions occur when photons are absorbed by the atom emitting an electron of the same energy (less the electron binding energy). Compton scattering occurs when a photon interacts with an atomic electron producing a scattered photon, a Compton recoil electron, and an antineutrino, all with a range of possible resulting energies which combine to equal the initial photon energy.

The fraction which is stopped within the counting gas is a function of the photoelectric absorption or scattering cross sections. These attenuation coefficients are published in various references (40). These coefficients depend on the element, type of interaction and energy of the photon. The fraction of photons which interact by a specific process within the detector is given by

$$f_{s_\gamma} = [1 - \exp(-(\mu/\rho)_j \rho\chi)] [\sigma j/\mu] \qquad (2.7)$$

where

(μ/ρ) = Cross section for any interaction

σj = Cross section for the specific interaction (ie. Photoelectric, τ/ρ, in this case)

Reduction Factor for Charged Particle Escape. Charged particles emitted from internal sources, particularly electrons, travel well-defined distances for different media and conditions. This stopping power data for different media, for several charged particles and for a range of particle energies is published in various sources. These distances are called the particle's range or residual range. Those charged particles which do not deposit all their energy are simply taken as one-fourth of those particles emitted within "their residual range" of the detector wall. The one-fourth reduction factor reflects the fact that not all of these particles are emitted radially outward. The fraction of particles escaping from internal gas sources in cylindrical detectors is then one-fourth the ratio of the annular volume (one residual range from the counter wall) to the total sensitive volume. This fraction is given by

$$f_{max} = \frac{\pi\, b^2 l - [\pi\, (b-R)^2\, (1-2R)]}{(\pi\, b^2 l)} \cdot \frac{1}{4} \qquad (2.8)$$

where

f_{max} = fraction of decays which do not deposit all of their energy

b = counter (cathode) radius

l = counter length

R = particle range

Since the fraction of particles stopped, f_s, is simply the fractional losses subtracted from unity. The former can be rearranged to give

$$f_{s_{e-}} = \frac{(b-R)^2\, (1-2R)}{4b^2 l} + 0.75 \qquad (2.9)$$

Gas Multiplication in Proportional Counters

Ionizing radiation can be efficiently detected in gas filled detectors. These detectors can be operated at voltages which produce signals proportional, but several orders of magnitude larger than that caused by the initial ionization. The phenomenon of gas multiplication produces this effect and can be quantified from theoretical relationships.

Gas Filled Detectors. Focusing on gas filled detectors, several different detectors result by varying the fill gas and the operating voltage applied to the device to collect the ion pairs. Five regions are noted. When minimum voltage is applied to collect all charges, the device is called an ion chamber. The next higher voltage region is where current is proportional to the initial ionization, but may be increased by a factor of one hundred to one thousand, or more. A detector operating in this region is called a proportional counter. The next three regions are of less interest. They are the regions of limited proportionality, the Geiger-Mueller region (where charge collected is independent of the ionization initiating it), and finally, the region of continuous discharge (51:303). See Figure 2.1 (33:40).

Gas Multiplication. The proportional counter is characterized by the phenomenon of gas multiplication to amplify the charge represented by the original ion pairs created within the gas. Gas multiplication is a consequence of the electric field of the detector (35:182). At low values of the electric field, electrons and ions drift to their respective collecting electrodes. Significant recombination occurs initially when the electric field is not strong enough to separate the ion pairs before this reaction occurs. During this transit

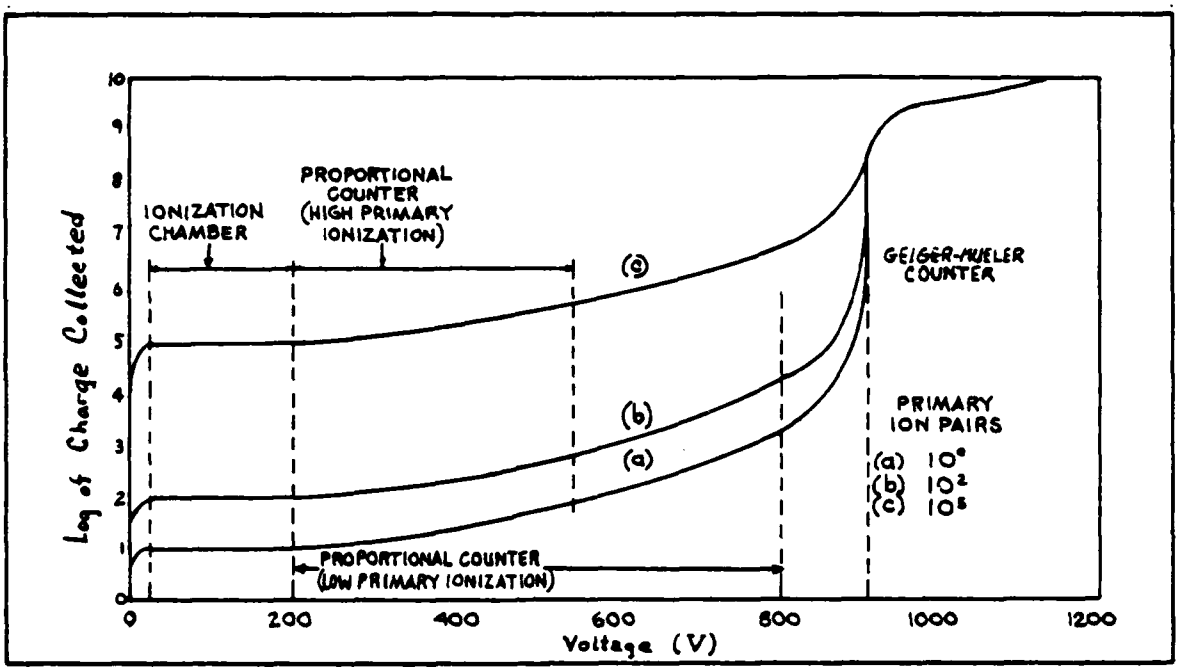

Figure 2.1. Voltage Regions for Gas Filled Detectors (33:40).

time many collisions occur with gas atoms, and ions gain very little kinetic energy between these collisions. Electrons, on the other hand, are more easily accelerated in the electric field and achieve significant kinetic energy between collisions, being nearly two thousand times less massive than the smallest monoatomic ion. The average electron kinetic energy between collisions increases with the electric field. As the electric field is increased above a threshold value (unique to each fill gas), the accelerating electrons achieve kinetic energies which exceed the ionization energy of the neutral gas atoms or molecules. When an electron with this kinetic energy collides with a gas atom, an additional ion pair is created. Typical gases at atmospheric pressure have threshold values for the electric fields on the order of one million volts/meter (35:183). The electron from this secondary

ionization will also be accelerated by the electric field. If sufficiently distant from the anode, this secondary electron can achieve kinetic energies sufficient to generate additional ionization via collisions with neutral gas atoms. This cascading process is known as the Townsend avalanche. The avalanche terminates when all free electrons have been collected at the anode. Over some region of the electric field, the collected charge will be proportional to the number of original or primary ion pairs created by the incident radiation. This voltage region has been labeled the proportional region and is the operational range for proportional counters.

Voltages Above the Proportional Region. Increasing the electric field above the proportional region can introduce non-linear effects. Although the electrons are greatly accelerated and are quickly collected at the anode, the positive ions which are at a minimum several thousand times more massive, move slowly through the fill gas towards the cathode. During the time required to collect all electrons generated, ion movement can be relatively insignificant. Therefore, each additional avalanche can add to a cloud of slowly drifting positive space charge. This space charge directly alters the electric field and indirectly changes the gas multiplication which is dependent upon the size of the electric field. Non-linearity between the operating voltage and gas multiplication results. At still higher voltages the fill gas becomes saturated with positive ions, reducing the electric field below the threshold where additional gas multiplication can occur.

Optimal Geometry for Intensifying the Electric Fields. Gas multiplication requires large values of the electric field. Cylindrical

geometry is frequently used for proportional counters where fields close to a central anode wire can be greatly intensified for a given applied voltage. From electrostatics the electric field at a radius r for cylindrical proportional counters is given by (35:185):

$$\vec{\varepsilon}(r) = V_b/(r \ln(b/a)) \qquad (2.10)$$

where

$\vec{\varepsilon}$ = electric field

V_b = voltage applied

a = anode radius

b = cathode radius

Large values of the electric field occur near the anode where r is small. For example, a cathode diameter of 5 cm and an anode diameter of 0.01 cm will create an electric field in excess of 3 million volts/meter near the surface of the anode when a 20 kV voltage is applied.

Quantifying Gas Multiplication Factors. The number of ion pairs produced in a cylindrical proportional counter per primary ionization event, the multiplication factor, can be quantified. First, the number of initial ion pairs can be calculated from the energy deposited in the absorbing material (fill gas) and from the average energy for production of an ion pair:

$$n_o = E_{dep} / W \qquad (2.11)$$

where

n_o = number of initial ion pairs

E_{dep} = energy deposited

W = average energy for the production of an ion pair

As the initial or primary electrons drift toward the anode, the

electric field increases as described above (as the radius approaches zero). When the field strength exceeds the threshold value, the Townsend avalanche occurs. The total charge produced is

$$Q = n_o \cdot M \cdot e \tag{2.12}$$

where

Q = total charge
M = multiplication factor, (proportional to $\vec{\varepsilon}(r)$)
e = charge per electron

Knoll (35:192) described the mean amplification factor as the integral of the first Townsend coefficient for the gas over the distance travelled. This coefficient is the mean number of secondary electrons produced by a free electron per centimeter of path travelled. The mean amplification factor, M, can be written

$$\int_{M(a)}^{M(r_t)} dM(r)/M(r) = \int_{a}^{r_t} \alpha(r)\, dr \tag{2.13}$$

where

$\alpha(r)$ = first Townsend coefficient
r_t = radius from the anode where $\vec{\varepsilon}(r)$ is below the threshold

Alpha is a function of the gas type and the magnitude of the electric field. Figure 2.2 depicts the first Townsend coefficients for noble gases.

The limits of integration can be changed such that the integral is explicitly a function of the electric field

$$\int_{M(a)}^{M(r_t)} dM(r)/M(r) = \int_{\vec{\varepsilon}(a)}^{\vec{\varepsilon}(r_t)} \alpha(\vec{\varepsilon})\, (dr/d\vec{\varepsilon})\, d\vec{\varepsilon} \tag{2.14}$$

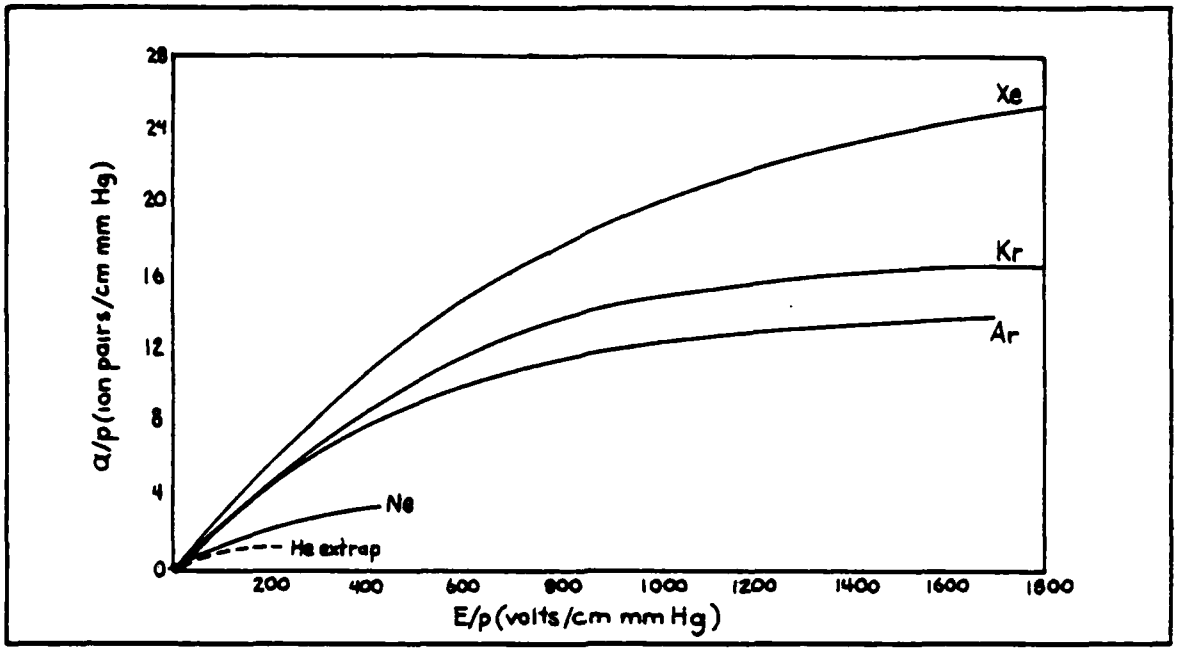

Figure 2.2. First Townsend Coefficients for Noble Gases (4:103).

By introducing equation (2.10) for the electric field in a cylindrical proportional tube, the multiplication factor can be rewritten as

$$dr/d\vec{\varepsilon}(r) = (-V_b / \ln(b/a)) \cdot (1/\vec{\varepsilon}^2(r)) \tag{2.15}$$

Substituting equation (2.15) into equation (2.14) gives

$$\int_{M(a)}^{M(r_t)} dM(r)/M(r) = \int_{\vec{\varepsilon}(a)}^{\vec{\varepsilon}(r_t)} \alpha(\vec{\varepsilon}) \cdot \frac{-V_b}{\ln(b/a)} \cdot \frac{d\vec{\varepsilon}}{\vec{\varepsilon}^2(r)} \tag{2.16}$$

This can be written

$$\ln M = \frac{V_b}{\ln(b/a)} \int_{\vec{\varepsilon}(a)}^{\vec{\varepsilon}(r_t)} \frac{\alpha(\vec{\varepsilon})}{\vec{\varepsilon}(r)} \cdot d \ln\vec{\varepsilon}(r) \tag{2.17}$$

For low values for the $\vec{\varepsilon}(r)/P$ ratio, the first Townsend coefficient can be approximated by assuming a linear relationship with respect to the electric field for a given pressure

$$\frac{\alpha(r)/P}{\vec{\varepsilon}(r)/P} = \frac{1}{\Delta V} \tag{2.18}$$

where

ΔV = constant, unique to each fill gas, which is proportional to the potential through which an electron moves between ionizing events.

Further, assuming the threshold value of the electric field is specified as

$$\vec{\varepsilon}(r_t)/P = K \tag{2.19}$$

where

K = minimum $\vec{\varepsilon}(r)/P$, below which multiplication cannot occur

Diethorn has derived the following relationship for multiplication factors based on the last two assumptions (35:193).

$$\ln M = \frac{V_b}{\ln(b/a)} \cdot \frac{\ln 2}{\Delta V} \cdot \left[\ln \frac{V_b}{P\ a\ \ln(b/a)} - \ln K\right] \tag{2.20}$$

Different simplifying assumptions have been made by other researchers, which produced somewhat different forms than shown in the Diethorn equation. A comparison of several of these different forms indicated Diethorn's equation was accurate over a wide range of operating conditions (11:97).

Figure 2.3 illustrates the influences of fill gas selection, counter bias, and operating pressure on the multiplication factor.

Characterizing the Pulse

The population of electrons and charged ions from the original

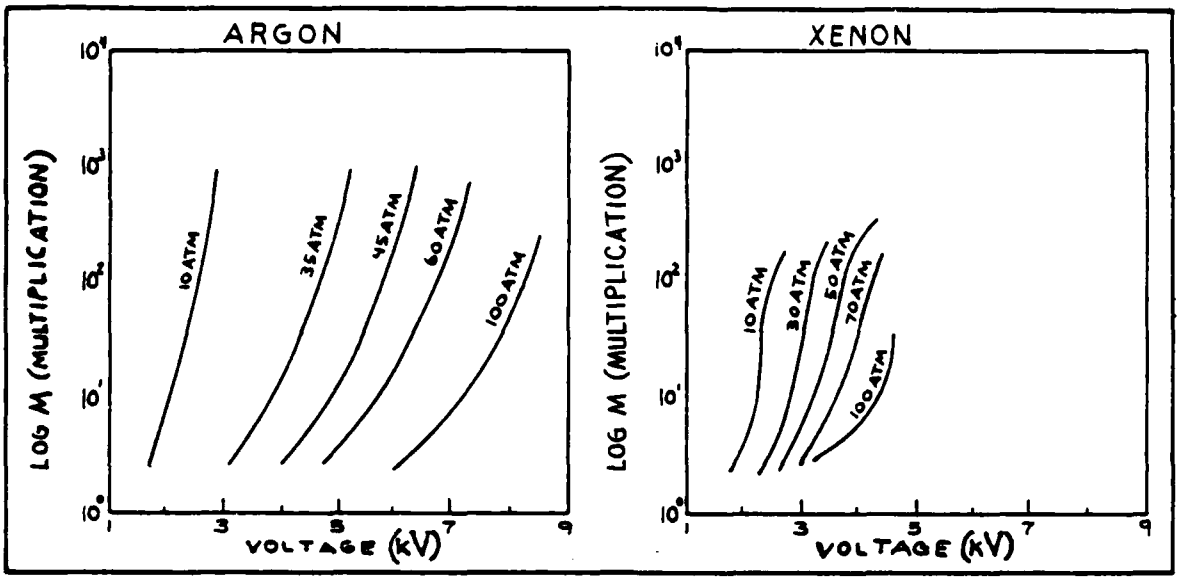

Figure 2.3. Pulse Amplification for Argon (left) and Xenon (right) for various voltages and pressures (19:1226; 43:828).

ionizing radiation is significantly increased by ion pairs produced in the Townsend avalanche. These charges are separated and collected at the anode and cathode, developing a change in the potential of the electric field. A signal pulse from the anode to the preamplifier occurs when the field is returned to its original potential. The time required to collect these charges and the characteristics of the pulse depend on the transport of the electrons and positive ions. Several competing processes reduce the quality and magnitude of the output signal.

Collection Time. While electrons are quickly collected at the anode, the full collection of the total charge does not occur until the more massive positive ions, produced in a sheath near the anode wire, drift to the cathode wall. The time required to collect the positive ions is found by

$$V_+ = \frac{dr_+}{dt} = \frac{\mu_+ \vec{\varepsilon}(r_+)}{P} \tag{2.21}$$

where

V_+ = average drift speed of the positive ions

μ_+ = positive ion mobility

r_+ = radial position of positive ion from central anode wire

Using the relation for the electric field in equation (2.10), separating the variables, and applying the appropriate limits, results in

$$\int_a^{r_+} r\, dr = \frac{\mu_+ V_b}{P \ln (b/a)} \int_0^{t_+} dt \tag{2.22}$$

Performing the integration and substituting the cathode radius b for the positive ion position at the time of collection yields

$$t_+ = \frac{(b^2-a^2)\, P \ln(b/a)}{2\mu_+ V_b} \tag{2.23}$$

For example, a 9.3 millisecond collection time results when a cylindrical counter (b = 2.5 cm, a = 25 μm) filled with argon gas (at STP) is operated with a 1700 volt cathode bias.

The transit time for electrons, calculated in a similar manner, is on the order of a few microseconds. This would require average electron drift velocities on the order of a few centimeters per microsecond. Experimentally measured electron drift velocities, presented in Figure 2.4, verify these expected values for two typical fill gases, argon and xenon.

Pulse Shape. The time history of the output pulse begins with the characteristic time for the transport of the primary electrons. This transit time can be divided into two stages. The largest part

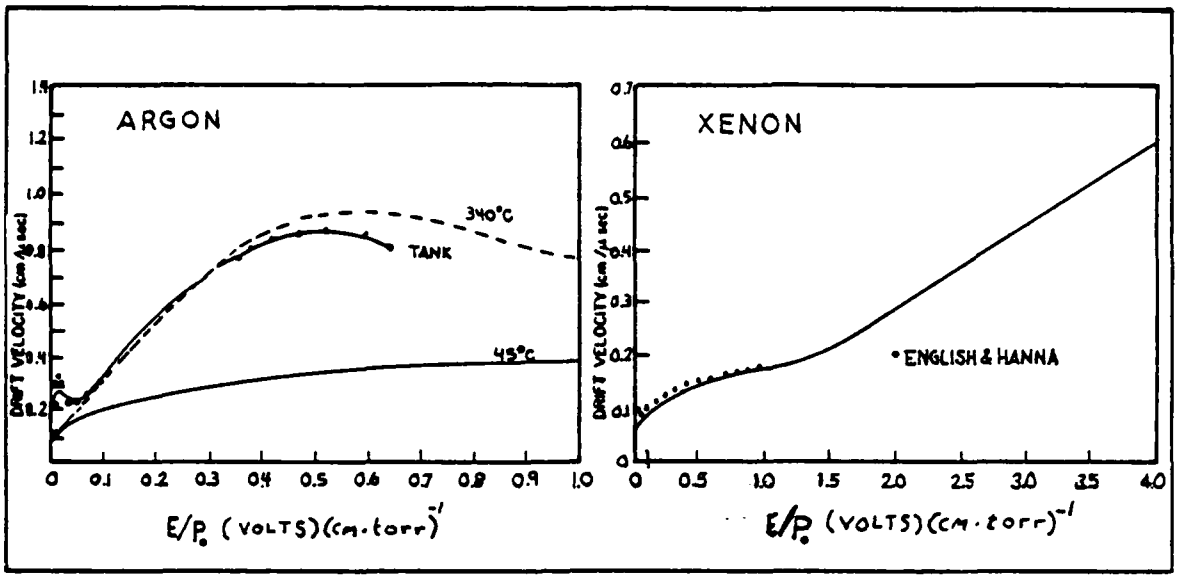

Figure 2.4. Electron Drift Velocities for Argon (left) and Xenon (right) fill gases at 680 torr and 267 torr, respectively (9:1413-1414).

of this time is associated with the drift time (~ microseconds) required for primary electrons to travel from their initial positions to a region a few mean free path lengths from the anode, where multiplication takes place. The second time component is the multiplication time required from onset to completion of the avalanche.

Drift. The potential change during the drift time is negligible compared to the contribution from the larger number of charge carriers formed in the subsequent avalanche. Drift time essentially introduces a delay time between formation of the initial ion pairs and the start of the output pulse.

Rise Time. Both primary and secondary electrons in the avalanche region are immediately collected, while the high intensity of the electric field rapidly propels the sheath of positive ions away from the anode toward the cathode. This results initially in a quickly

rising signal pulse. As the positive ions are transported to greater radii where the field is smaller, the later part of the pulse rises more gradually. Normally finite shaping times of supporting electronics equipment cut off most of the latter component of the signal (35:203).

Calculation. The pulse shape described by Wilkinson (55:17) and modified by Richer and Groves (24:227) is formulated as

$$\frac{V_a(t)}{V_{max}} = B \ln (1 + {}^{t}/_{t_a}) \tag{2.23}$$

where

$V_a(t)$ = change in anode voltage across resistance in counter circuit (R_L in Figure 2.5).

V_{max} = characteristic voltage associated with the stored charge (after collecting all charge carriers) where the proportional tube acts as a capacitor (as specified in equation (2.24), below).

B = characteristic constant of the proportional counter (see equation (2.25), below).

t = time from start of the multiplication process

t_a = a characteristic time associated with the counter, derived from equation (2.23), and specified in equation (2.26), below.

The characteristic constants are given by

$$V_{max} = \frac{Q}{C} = \frac{n_o e M}{C} \tag{2.24}$$

where

C = capacitance of the proportional tube

and

$$B = (2 \ln(b/a))^{-1} \tag{2.25}$$

$$t_a = \frac{a^2 P}{2 V_b \mu_+ \ln(b/a)} \tag{2.26}$$

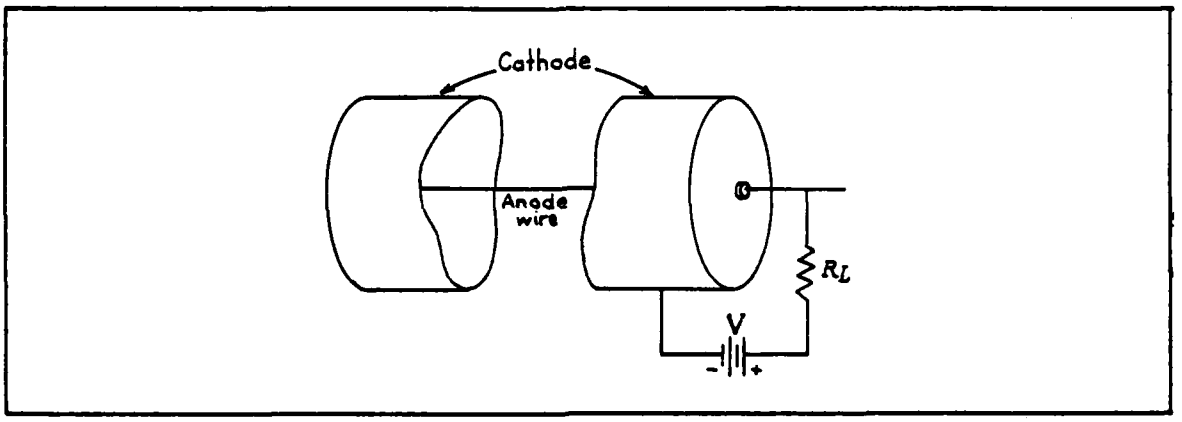

Figure 2.5. Circuit Diagram for Proportional Counter (35:185).

Fast Pulses. Fast output pulses are thus promoted by high voltages and small anode wires, which result in large electric field values. Higher pressures, as expected, increase the characteristic time.

Variance. Ion pairs have a range of original positions or radii, and develop a spread in the rise time characteristics of the pulse. Figure 2.6 shows the shape of the expected leading edge of the output pulse for two fill gases, under two sets of conditions: ion pairs formed at a constant radius (solid lines), and ion pairs uniformly distributed throughout the volume of the counter (dashed lines).

Effects Which Reduce Signals. Several effects change the time characteristics or the magnitude of the output signal by altering the axially uniform electric field and upsetting the proportionality of the multiplication process. End effects and eccentricity of the anode wire produce these effects. Likewise, self-induced or general space charges from high densities of positive ions can modify expected signals.

Other effects change the signal by reducing primary electrons or by increasing late emissions of secondary electrons. These effects may result from recombination problems in the former case, and by

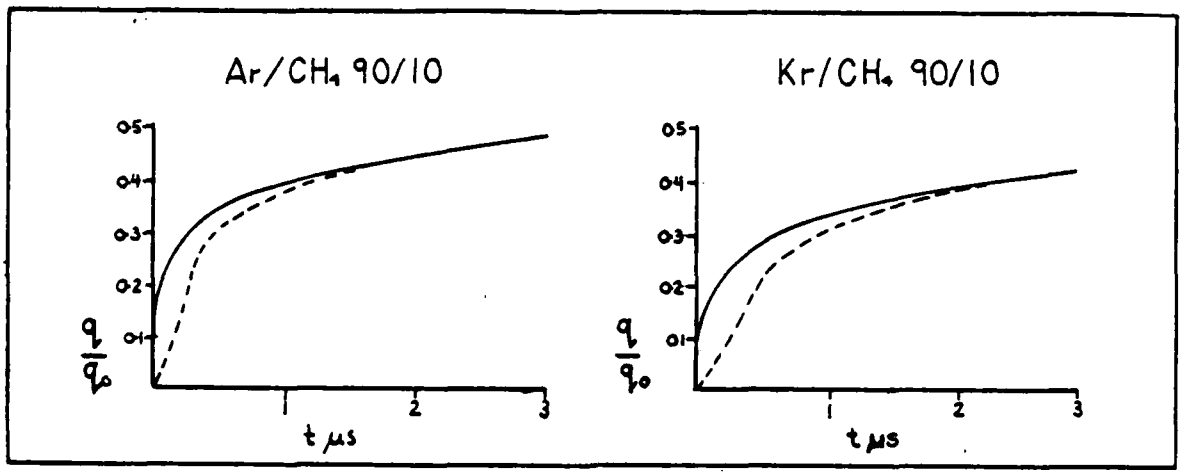

Figure 2.6. Proportional Counter Pulse Shape for Two Different Fill Gases. Solid curves represent initial ionization formed at single radius (constant drift time), and dashed curves represent uniform ionization throughout sensitive volume of counter (12:159).

spurious or after pulses from various sources in the latter case.

Anode Wire Variance. The quality of the output signal depends on a high degree of local proportionality in the Townsend avalanche. Each electron formed must undergo the same amount of gas multiplication. This factor can be upset with distortions to the axially uniform electric field. Variations to the wire diameter, eccentricity of the wire position or particulates attached to the wire produce nonuniformities in the field. Primary electrons thus undergo different degrees of multiplication. This consequence can be understood from the Diethorn relation, equation (2.20). Variation of the electric field due to eccentricity of the wire (Δ) is given by (47:95)

$$\delta\vec{\varepsilon}/\vec{\varepsilon} = 4\ a\Delta/b^2 \qquad (2.27)$$

Irregular fields, caused by particulates on the wire itself, are easily corrected. This is accomplished by a simple process of electrically glowing the anode wire, when the detector is evacuated (37:198).

End Effects. End supports and end caps can cause similar distortions to the electric field. These end effects also result in variations in the multiplication process near the ends of the anode wire. Small diameter field tubes, which extend from the end plates a distance equal to the cathode radius, shield the ends of the anode. The field tubes are adjusted to the appropriate potential relative to their radial position and collect primary electrons formed near the ends of the counter. The field tube potential is determined from a relation derived from equation (2.10) (14:39)

$$V_f/V_b = \ln (r_f/a) \; / \; \ln(b/a) \qquad (2.28)$$

where

V_f = field tube potential or bias

r_f = field tube radius

Space Charges. Self-induced charge and general space charge from dense positive ion populations near the anode wire alone or throughout the sensitive volume, alter the multiplication factor and resultant signal. Self-induced effects result from high multiplication factors which produce an abundance of positive ions in a sheath near the surface of the anode. These ions disturb the electric field. Conversely, at high rates of primary ion pair formation, related to the activity of the radioactive source, the density of drifting positive ions is increased throughout the detecting media. This general space charge produces non-linearities in the electric field as the ions gradually drift toward the cathode. Effective potentials can be calculated (10:224). Both types of ion charge effects are minimized using sources of moderate activities and voltages which produce acceptable multiplication factors (below 100).

Recombination. The charge collected can be reduced by recombination of the ion pairs which directly alters the output signal. Different types of recombination may occur depending upon the ionization density, the electric field and the mobility of the electrons. Randon or diffusive recombination occurs where small gas stopping powers or low fields are involved. Alternately, columnar recombination occurs where large gas stopping powers are involved and is directly related to the orientation of the path of the radiation quanta with respect to the orientation of the electric field. Experimental evidence suggests that columnar recombination is not negligible at high pressures between heavy ions. Jaffe's theory (46:303) of this process has been employed to correct for these effects, but is not appropriate where large differences in drift velocities exist. Disassociative recombination involving certain polyatomic gases usually has large recombination coefficients (between 10^{-6} and 10^{-8} cm^3/sec). Other forms include radiative, dielectric and three body recombination effects. These are normally considered lessor effects (with coefficients from 10^{-10} to 10^{-12} cm^3/sec). However, with low electric fields and high pressures, recombination effects become more severe.

Recombination from impurities. The characteristics of the detecting gas including the electronegativity of the gas or impurities can also affect recombination. Electron attachment is the major concern for this system and occurs as a result of electronegative impurities in the fill gas. After an electron is captured by an electronegative impurity, it is easily recombined with a positive ion. The mean free path length for electron attachment is of the form

$$\lambda_{ath} = \alpha_{ath} \vec{\epsilon} / C_i \qquad (2.29)$$

where

α_{ath} = attachment proportionality constant

C_i = concentration of impurities.

In addition to reducing the output signal, electron attachment also causes a position dependence. Oxygen, nitrogen and water vapor are the major impurities of concern in this research. Further discussions in the following chapter describe purification processes available.

Spurious and After Pulses. Photon radiation emitted by the de-excitation of fill gas molecules can interact with the cathode. Also, collisions between positive ions or neutral atoms and the cathode wall may produce spurious or after pulses. Both of these interactions result in the emission of electrons following the avalanche process of the primary electrons. If allowed to occur, these after pulses can be self sustaining or can produce continuous discharges in the extreme case. Additives of polyatomic gases or noble gas mixtures can reduce this effect and are discussed further in Chapter III.

Energy Resolution. The effects which alter the detector's output signal cause a spread in the observed pulse amplitude distribution degrading the resolution of the recorded spectra. Energy resolution is a measure of the proportional counter's ability to detect fine details in the spectra. It is normally expressed by the full width at half the maximum height (fwhm) of a peak in a pulse height distribution spectrum. Statistical considerations of the variance of primary ion pairs, and, of the avalanche caused by a single electron, serve to specify the limiting case for resolution. Other fluctuations such as circuit noise affect resolution (35:203). Since pulse amplitude is proportional to

the total charge collected, the variation in the pulse is related by equation (2.1) as follows

$$\left(\frac{\sigma_Q}{Q}\right)^2 = \left(\frac{\sigma_{n_o}}{n_o}\right)^2 + \left(\frac{\sigma_m}{M}\right)^2 \tag{2.30}$$

Variance in Amplification. The variance of the single-electron multiplication factor A and the average multiplication factor M is given by

$$\sigma_m^2 = \frac{1}{n_o}\,\sigma_A^2 \tag{2.31}$$

and substituting into equation(2.30),results in (35:197)

$$\left(\frac{\sigma_Q}{Q}\right)^2 = \left(\frac{\sigma_{n_o}}{n_o}\right)^2 + \frac{1}{n_o}\left(\frac{\sigma_A}{\bar{A}}\right)^2 \tag{2.32}$$

Variance in Primary Ion Pairs. The relative variation in the original ion pairs is expressed in terms of a Fano factor, F, where

$$\sigma_{n_o}^2 = F\,n_o \tag{2.33}$$

where values for this factor range from 0.05 to 0.20 (20:47).

The variance of the multiplication factor as predicted by Polya distribution is

$$\left(\frac{\sigma_A}{\bar{A}}\right)^2 = \frac{1}{\bar{A}} + b \tag{2.34}$$

where observed values of b are about 0.5 (35:199). Where the multiplication factor $\bar{A}$ is sufficiently large

$$\left(\frac{\sigma_A}{\bar{A}}\right)^2 \simeq b \tag{2.35}$$

Overall Statistical Limit. The statistical limit for large values of primary ion pairs ($n_o \gtrsim 20$) approaches a Gaussian distribution. This allows the relative standard deviation of the pulse amplitude distribution from equation (2.32) to be given by (52:251)

$$\left(\frac{\sigma_Q}{Q}\right) = (F + b / n_o)^{0.5} \tag{2.33}$$

or substituting with equation (2.1), yields

$$\left(\frac{\sigma_Q}{Q}\right) = (W (F + b) / E_{dep})^{0.5} \tag{2.34}$$

Where all energy of the radiation quanta is deposited, assuming normal pulse height distribution, this variance can be expressed in terms of the more conventional fwhm.

$$\left(\begin{matrix}\text{fwhm} \\ \text{E-Limit}\end{matrix}\right)_{det} = 2.36 \left((F + b) E_{dep} W \right)^{0.5} \tag{2.35}$$

Other Resolution Factors. Other contributions to energy resolution can also be expressed in the form of a fwhm_i, provided each contribution is independent of the others and the effects are additive and randon (35:201), as below

$$\text{fwhm}_{ph} = \left[(\text{fwhm})^2_{det} + (\text{fwhm})^2_{noise} + (\text{fwhm})^2_i \text{ ---} \right]^{0.5} \tag{2.36}$$

where the subscripts are defined as

ph = pulse height amplitude
det = limiting detector variance
noise = variance from circuit noise
i = other independent, additive and random effects.

Design Considerations and Resolution

The efficiency and resolution of the high pressure proportional detector have thus far been shown to be a consequence of the radiation quanta and the operating conditions which influence the multiplication process. Likewise, the dimensions of the detector, the size of the wire, and the size of the field tube affect the multiplication process as illustrated in the Diethorn relation, equation (2.20). Table 2.1 lists some examples of limiting resolutions for various counting gases. These influences are discussed in detail in the next chapter.

Table 2.1

Resolution Related Constants for Proportional Counters

Fill Gas	w-value (eV/ip)	Fano Factor(F) Calc.	Fano Factor(F) Exp.	Multiplication Variance(b)	fwhm at 5.9 keV Calc.	fwhm at 5.9 keV Exp.
Ne	36.2	0.17		0.45	14.5%	
Ar	26.2	0.17		0.50	12.8%	
Xe	21.5		≤.17			
Ne-Ar (99.5%-0.5%)	25.3	0.05		0.38	10.1%	11.6%
Ar-C_2H_2 (99.5%-0.5%)	20.3	0.075	≤.09	0.43	9.8%	12.2%
Ar-CH_4 (99.2%-0.8%)	26.0	0.17	≤.19			
Ar-CH_4 (90%-10%)	26.0			0.50	12.8%	13.2%

(35:201)

III. Fill Gases and Radioactive Sources

Introduction

With a stable high voltage supply and a specific gas pressure, the operating characteristics of the detector are determined by the selection and purity of the counting gas. The operating voltage and gas pressure's influence on the gas multiplication factor can be seen from the Diethorn relation in the preceding chapter, equation (2.20). This directly correlates the detector's response to ionizing radiation. Likewise, small changes in the composition of the fill gas or additions of electronegative impurities significantly alter the detector's operating characteristics.

It is for this reason that high pressure proportional counters are calibrated with x-ray and gamma sources using purified counting gases of known composition. The advantage of using collimated beams from these sources to initially determine the detector's response is that their characteristic energies do not change as they pass through the wall of the detector. These radiations give rise to photoelectrons of well-defined energy. The inherent width of the photon energy distribution is small compared with the energy resolution of the detector. Therefore, a measurement of the detector's response is more correctly related to its own limiting resolution, rather than any variation in the incident gamma ray energy.

After these calibration sources are used to examine various aspects of the detector's response, the more complex decay schemes of the radioactive noble gas sample are analyzed. Though atmospheric releases of radioactive noble gases may reasonably include numerous

xenon isotopes and isomers, the effects of radioactive decay reduce such a sample to two principal radioisotopes, ^{131m}Xe and ^{133}Xe.

The detector's response to the test sample can be predicted in the form of a combined pulse height spectrum by considering the expected detector resolution, the detector's efficiency, the fill-gas physical characteristics, and the nuclear decay data of these remaining xenon radioisotopes.

This chapter presents some of the more significant physical characteristics and considerations of the fill gases. Secondly, principal decay schemes of the external gamma sources, used for calibration, are discussed. Next, the time history of a typical atmospheric sample of a radioactive noble gas release is analyzed. Finally, the expected response of the high pressure proportional counter to the proposed radioactive xenon test sample is presented.

Detecting Gases

Since gas multiplication is critically dependent upon the migration of free electrons rather than negative ions, detecting gases for proportional counters must have minimal electron attachment coefficients. Noble gases and certain others undergo no electron attachment and offer other important characteristics which make their use as fill gases ideal. Argon, the most abundant noble gas in the atmosphere, and xenon, the rarest stable noble gas, are both available in 99.999% ultra-pure form. Electronegative impurities such as oxygen, even in the parts per million range, significantly alter the signal-to-noise response in high pressure proportional counters. Getters used in purification processes can reduce this problem. However, even with highly

purified noble detecting gases, gas multiplication factors which exceed one hundred may exhibit instabilities or proportionality fluctuations caused by the propagation of ultraviolet photons. Minimal additions of polyatomic organic quench gases can reduce this erratic behavior (53:389).

Noble Gases. Negative ion formation readily occurs in electronegative elements such as the halogens and oxygen, but in other gases very little occurs. Included in the latter group, in addition to the noble gases, are hydrogen, carbon monoxide, carbon dioxide and methane, among others (45:584). The noble gases, as opposed to the listed polyatomic gases, are widely used as the principal components for fill gases because of greater stopping power and high intrinsic efficiencies.

Helium and argon are generally the most frequently used noble gases, while krypton and xenon, the heaviest stable noble gases, offer greater stopping power and increased photon interactions. However, krypton and xenon are extremely expensive due to their relative scarcity. Helium, the second most abundant element in the universe, and all other inert gases associated with earth, are generally occluded in rocks or dissolved in water rather than comprising a significant component of the earth's atmosphere.

While argon makes up nearly one percent of the atmosphere, all other rare gases combined total less than 0.003%. None-the-less, with the exception of helium, noble gases are produced by liquefaction of air and separated into components by fractional distillation. Helium, the single exception, is principally extracted from vapor deposits associated with a limited number of oil fields.

Table 3.1 compares selected noble gas physical data. It should

be noted that three of the five stable inert gases are readily liquefied and solidified by normal low temperature methods. Helium and neon are the exceptions. The required use of liquid nitrogen (boiling point 76.4°K) for cryogenic pumping in this research makes these characteristics significant.

Table 3.1

Comparison of Selected Noble Gas Characteristics

Noble Gases	Atomic[a] Weight	Dry Air[b] Vol. Percent	Triple[a] Point (°K)	Boiling[a] Point (°K)
He	4.0026	5.2×10^{-6}	None	4.22
Ne	20.183	1.8×10^{-5}	24.55	27.07
Ar	39.944	0.93	83.81	87.27
Kr	83.80	1.1×10^{-6}	115.95	119.80
Xe	131.30	8.6×10^{-8}	161.39	165.05
Rn	(222)	6.0×10^{-20}	(202)	(211)

([a] 30:392-393; [b] 54:4)

Argon and Xenon. Though a limited quantity of 99.999% ultra-pure xenon was available, 99.999% ultra-pure argon was used throughout the research because of its relative availability and minimal expense. However, both gases are characterized to support further discussions in subsequent chapters.

Argon fill gas consists almost entirely (99.6%) of a single isotope, ^{40}Ar, whereas xenon is a mixture of several different isotopes. Table 3.2 lists the relative abundances of stable argon and xenon isotopes in the atmosphere.

Table 3.2

Relative Isotopic Abundances of Argon and Xenon from Atmospheric Samples

Noble Gas	Mass Number	Relative Isotopic Abundance (Mole %)
Ar	36	0.337
	38	0.063
	40	99.600
Xe	124	0.096
	126	0.090
	128	1.919
	129	26.440
	130	4.080
	131	21.180
	132	26.890
	134	10.440
	136	8.870

(54:4)

Selected physical properties of these two noble gases are listed at Table 3.3. Additionally, vapor pressure data for argon and xenon are presented in Tables 3.4 and 3.5, respectively. Interpolation, between the vapor pressure data points listed, is accomplished using the Antoine equation of state, which has the following form (18:10-28).

$$\text{Log}_{10} P = A_a - B_a/(T + C_a) \qquad (3.1)$$

where

P = pressure [Torr]

T = temperature [°C]

A_a, B_a, C_a = Antoine equation constants unique for each gas

Table 3.6 lists the Antoine equation constants used for argon and xenon.

Table 3.3

Argon and Xenon Triple Point Data

Triple Point	Argon	Xenon
Temperature (°K)	83.81	161.39
Pressure (Torr)	517.1	612.2
Density		
Solid (g/cc)	1.622	3.54
Liquid (g/cc)	1.414	3.076
Vapor (mg/cc)	4.05	8.18

(25:111)

Table 3.4

Argon Vapor Pressure Data

Temp (°K)	Pressure (Torr)	Temp (°K)	Pressure (Torr)
66	26	78	226
68	39	80	305
70	58	82	405
72	84	84	531
74	119	86	661
76	165	90	1003

(26:326)

Table 3.5

Xenon Vapor Pressure Data

Temp (°K)	Pressure (Torr)	Temp (°K)	Pressure (Torr)
70	1.39×10^{-4}	120	11.5
80	4.24×10^{-3}	130	38.2
90	5.99×10^{-2}	140	101
100	4.95×10^{-1}	150	258
110	2.76	160	562

(27:800)

Table 3.6

Antoine Equation Constants for Argon and Xenon

Element		A	B	C
Ar	solid	7.50581	399.085	272.63
	liquid	6.61651	304.227	267.32
Xe	solid	7.4845	714.896	264.0
	liquid	6.64289	566.282	258.66

(18:10-29, 10-36)

A final consideration, when using these two noble gases at low temperatures or at high pressures, is that molecular volumes are no longer negligible and that attractive forces between molecules become significant. This deviation from ideal gas laws is illustrated in Figure 3.1. Van der Waal's equation was used for pressure and volume calculations, particularly when xenon was involved.

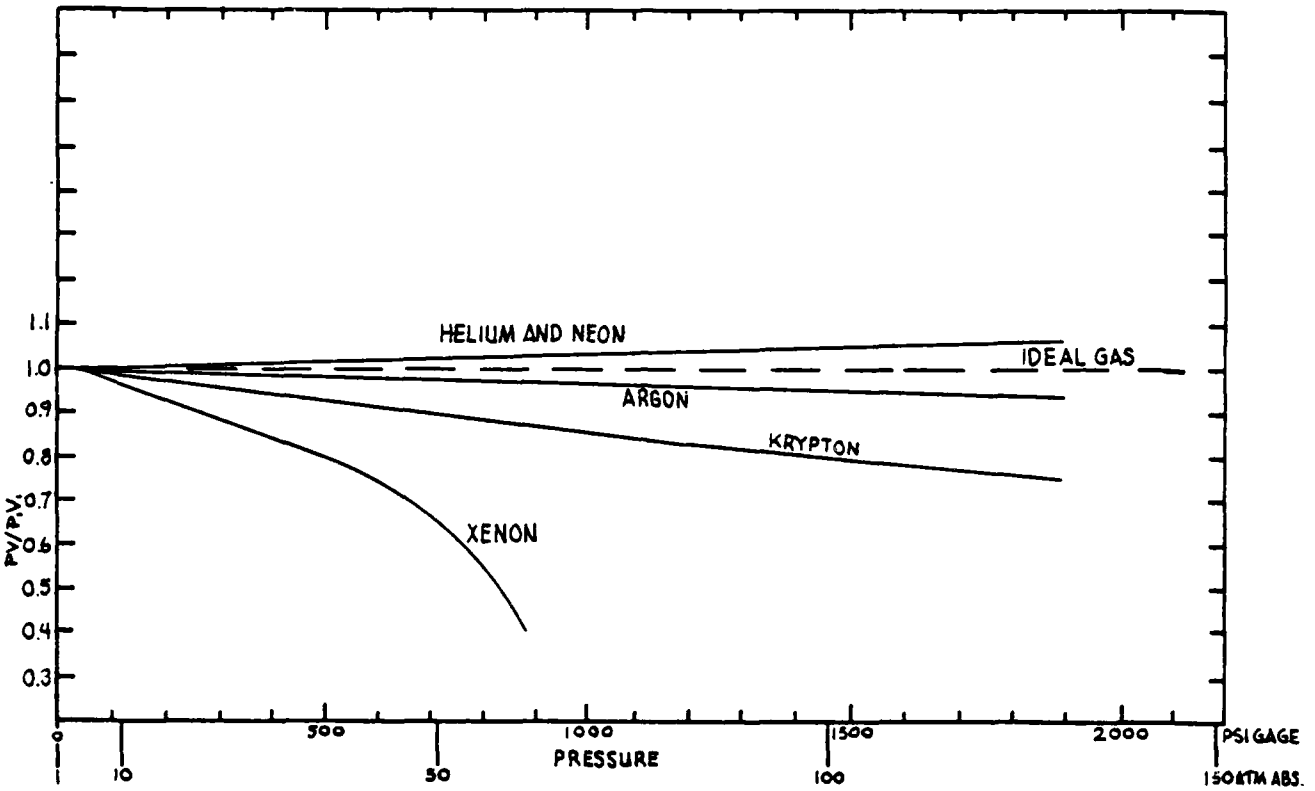

Figure 3.1. Compressibility of Inert Gases (15:241)

Purification Process. Though ultra-pure detecting gas is used, impurities in concentrations of a few parts per million are also included. Other impurities of this same magnitude are introduced through leaks and from releases of gases and water vapor adsorbed on the detector's inner surfaces. Several purification methods are available which reduce the electronegative impurities to an operational range of about ten parts per billion, or less (5 :1041). The counting gas used in this research was purified by flowing the gas through a quartz tube filled with zirconium and titanium turnings heated to 1000°C.

Ultra-pure detecting gases are nominally 99.996% to 99.999% pure. This includes 100-400 ppb impurities. Additional impurities enter the proportional counter through leaks, even when operated at high

pressures. Air enters the vessel by flow which is counter current to the outward escape of the inert gas. Although this counter flow is several orders of magnitude smaller than the flow rate of the inert gas, it is sufficient to introduce impurities over time in the 100 ppb range. Further, various gases and water vapor adsorbed on the inside surfaces of the counter are continuously released into the detecting media and can approach this same level of concentration (42:612).

Besides decreasing electron drift velocities, electronegative atoms and molecules at these concentrations can capture significant numbers of the primary electrons (44:367). Some of the more readily introduced impurities include atmospheric oxygen, water vapor, nitrogen, oxides of sulphur and the halogens. The effects of these impurities are exacerbated at higher pressures and with the use of the heavier inert gases. In collecting experimental data, these impurities cause counting plateaus to shift, counting stability to be adversely affected, and pulse height spectra to be reduced. In the limit, signal to noise ratios are altered to the extent that readable signals are lost in background noises.

In eliminating impurities, two related purification processes are available. Both methods involve the use of finely divided metals at elevated temperatures, which chemically react with the impurities forming product coatings on the surfaces of the metal reactants. The simplest approach is to introduce the gas into a chamber partially filled with heated metal particles allowing convection currents to complete the process. The second method is a dynamic process where a continuous flow of impure gas is directed through a chamber or tube containing the hot metal turnings.

Various metals are used as getters with different temperature ranges for each. Crosswhite and Dieke (17:433) recommended a highly active form of uranium, prepared by decomposing uranium hydride at 400°C for eliminating impurities. Another method for the removal of chemically active impurities in inert gases was described by Bennett (7:1092). He used a series of commercially available barium getters which were activated by heating for a few seconds just before passing the gas into the chamber. Bennett suggested that impurities were reduced from 10 ppm to 1.0 ppb in this process within a few minutes.

Gibbs, Svec and Harrington (22:289) compared fifteen different metals and alloys for the chemical purification of argon in flow systems. They stated that barium, calcium, magnesium, thorium, zirconium and an alloy of 90% calcium and 10% magnesium were satisfactory for removing both nitrogen and oxygen. They further suggested that the best metals for removing impurities at relatively low temperatures (300 to 500°C) were barium and the calcium-magnesium alloy. In the case of titanium-zirconium mixtures, oxygen and nitrogen are removed at 600°C and 1000°C, respectively.

Though requiring high temperature, Knapp (34) selected a flow through quartz purification apparatus using the titanium-zirconium mixture operated at 1000°C. Difficulties associated with this selection are addressed in the discussion of experimental results.

Quench Gases. Even after purifying the fill gas, operation of the detector at high pressures with large gas multiplication factors can cause instabilities which alter the proportionality required of the multiplication process. As already presented, the signal pulse is initiated when the avalanche of electrons arrive at the central

anode wire of the counter. Positive ions are accelerated toward the cathode wall and on impact with the wall may cause secondary electron emissions which do not correlate to the primary ionizing radiation. Other sources which may cause secondary electron emissions from the cathode wall include de-excitation photons from the fill-gas, and the collisions of neutral and meta-stable fill-gas atoms and molecules with the detector wall. Any of these sources may cause a variable number of signal pulses for a single ionizing event or, in the limit, continuous discharges. To prevent this unstable response, secondary emissions are quenched.

This is accomplished in fast proportional counting by adding certain heavy organic vapors as quench gases. Some gases used for this purpose include ethyl formate, ethanol, methane, carbon dioxide and others. The molecules of the organic vapor absorb energy from any of the various secondary sources, significantly reducing the liberation of electrons from the walls of the counter. More importantly, collisions between primary event electrons and quench gas molecules result in vibrational or rotational excitations in the quench gas molecules which de-excite by emission of low energy infra-red photons rather than the ultraviolet photon emissions associated with de-exciting meta-stable fill gas atoms.

Counters with quench gases added to the fill-gas become sensitive again after a period of 100 to 200 microseconds following the primary ionizing event (45:586). The polyatomic molecules absorb the energy from these interactions and are ultimately decomposed. The quenching properties of the gas are reduced with use and in time must be replaced.

Several researchers, including Pisarev et al. (43:830), have

suggested that the operation of proportional counters using a single noble gas even with a quench gas are inherently unstable at high pressures. They recommend using a mixture of noble gases in addition to a polyatomic quench gas. In addition, continuous purification of this detecting media during its use is described as a potential requirement at higher pressures.

Small concentrations of a second noble gas, often xenon, can significantly improve the characteristics of the primary noble detecting gas. The ionization energy of the added gas should be lower than both the ionization energy and the metastable energy levels of the principal gas. Thus, collisions between excited primary gas atoms and neutral additive atoms ionize the latter. Because the excitation energy would have otherwise been lost without the added gas, these improved ionization yields reduce gas multiplication fluctuations by as much as fifty percent (35:191).

Calibration Sources

With purified detecting gas of known composition at the appropriate pressure, external gamma ray sources are used to obtain precise energy and efficiency calibration data. Since the gamma rays emitted are nearly monoenergetic, the inherent photon energy distribution observed is directly related to the resolution of the detector as mentioned earlier.

These sources normally consist of samples of radioisotopes of a few microcuries encased in plastic discs. The thickness of the encapsulation is generally large enough to stop particulate radiations from the decay of the parent nucleus, and the radiation energy from

the source is the gamma radiation produced in the daughter decay. The gamma ray emission rate is sufficiently high to allow for absorption losses of the collimated beam through the detector wall.

Sources used to carry out accurate efficiency calibrations must have their absolute activity known or experimentally measured using a previously calibrated detector.

Three sources which were available included americium-241, cadmium-109 and cobalt-57 with their respective 59.54 keV, 88.03 keV and 122.01 keV gamma rays.

Americium-241 with a 432.2 year half-life decays by alpha emission to isomeric states of neptunium-237. Most decays (86%) result in excited states, 59.54 keV above the ground state. A gamma ray of this energy is emitted as neptunium-237* returns to the ground state (38:430). It has a branching ratio of 0.359.

In a similar manner, Cadmium-109 with its 453 day half-life decays by the process of electron capture to a metastable state of silver-109, 88.03 keV above the ground state. Characteristic silver gamma rays are emitted with a branching ratio of 0.0361 returning silver-109* to the ground state (38:250).

Finally, the cobalt-57 source with a 270.9 day half-life decays by electron capture principally (99.8%) to an excited state of iron-57, 136.32 keV above the ground state. Three primary gammas are emitted. A 136.32 keV gamma ray is emitted with a 0.106 branching ratio which returns the excited iron-57 to its ground state. A 122.01 keV gamma is emitted with a 0.856 branching ratio, which allows the excited iron-57 to drop to a lower excited state (14.31 keV above the ground state. Subsequent de-excitation to the ground state results in the emission of a 14.31 keV gamma with a 0.095 branching ratio).

Other x-rays, gamma rays and Auger electrons are emitted by these sources, but are too weak to penetrate the combined thicknesses of the source capsule and the detector wall; or they are excessively energetic such that they are not stopped within the sensitive volume of the detector. Decay schemes for these three sources at Figures 3.2 to 3.4 summarize this information.

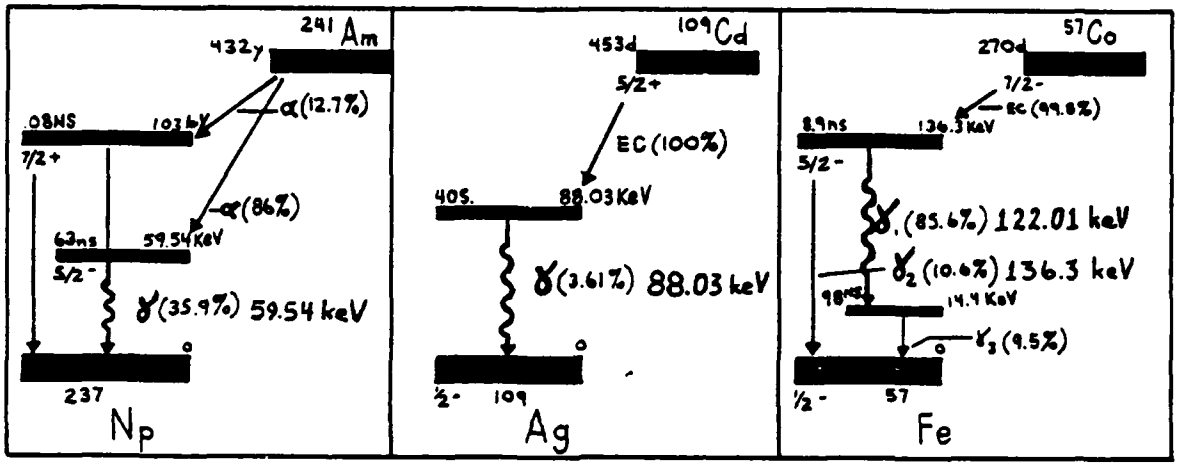

Figure 3.2. ^{241}Am Decay Scheme (38:430)

Figure 3.3. ^{109}Cd Decay Scheme (38:250)

Figure 3.4. ^{57}Co Decay Scheme (38:191)

Radioactive Xenon Sample

The radioactive noble gas sample is examined after various aspects of the detector's response and efficiency are determined using the calibration sources. Such an atmospheric sample of radioactive noble gases is most often associated with releases from nuclear power generating reactors. Secondary sources include naval propulsion reactors and nuclear weapon tests, among others. With the exception of radon, radioactive noble gases are predominantly a result of man's nuclear activities.

The types and activities of the radionuclides in releases vary by source and by operating history of that source. Regardless of source, xenon radioisotopes from such releases can be isolated through fractional distillation. As a result of the different decay rates, such a sample is reduced to two major radioisotopes of xenon.

Radioactive Noble Gas Releases. Though the composition of atmospheric noble gas releases may vary depending on source, xenon and krypton are the principal noble gases produced by nuclear fission. The remainder of this discussion will therefore focus on one specific example, fission yields from the thermal fissioning of uranium-235 (associated with releases from thermal reactors). Table 3.7 lists the significant yields of xenon isotopes from a thermal uranium-235 fission source.

A cursory inspection of this data could focus attention on certain higher yield radiosotopes, while ignoring others. However, over a period of hours and days, the contributions to total activity

Table 3.7

Xenon Yields from Thermal Fission of Uranium-235

Isotope	Half-Life	Yield(%)	Isotope	Half-Life	Yield(%)
131m	120 days	0.017	135m	15.7 min	1.05
131	*	2.77	135	9.2 hrs	6.72
132	*	4.13	136	*	6.12
133m	2.26 days	0.19	137	3.80 min	5.94
133	5.27 days	6.77	138	14.2 min	6.24
134	*	7.19	139	40.0 sec	4.96

(41:69) *-stable

of the sample is altered dramatically as a result of different decay rates. Table 3.8 presents the relative activity over time of the two principal radioactive noble gases from uranium-235 fission by thermal neutrons.

Table 3.8

Relative Activity (Over Time) of Radioactive

Noble Gas Samples From $^{235}_{U}$ Fission By Thermal Neutrons

		Fractional Activity (%) Over Time					
Isotope	Half life	2min	2hrs	3days	10days[a]	20days[a]	60days
^{139}Xe	41.0 sec	3.0					
^{89}Kr	3.2 min	8.2					
^{137}Xe	3.8 min	11.3					
^{135m}Xe	15.0 min	4.6	0.1				
^{138}Xe	17.0 min	14.1	0.3				
^{87}Kr	1.3 hrs	7.3	5.7				
^{83m}Kr	1.9 hrs	1.3	1.4				
^{88}Kr	2.8 hrs	10.2	13.5				
^{85m}Kr	4.4 hrs	4.2	6.7				
^{135}Xe	9.2 hrs	17.2	32.2	0.5			
^{133m}Xe	2.3 days	0.5	1.0	1.5	0.5	0.1	
^{133}Xe	5.3 days	18.0	30.0	96.7	96.4	90.8	2.5
^{131m}Xe	12.0 days	0.1	0.2	0.8	1.1	2.2	1.0
^{85}Kr	10.7 yrs	0.1	0.1	0.5	2.0	6.9	96.5

(13:76) (a) Interpretation of data otherwise listed.

The effects of natural decay reduce the significant activity contributions of the radioactive noble gases to Krypton-85 and two radioisotopes of xenon. With a thirty degree (°C) separation in boiling point temperatures, the xenon radioisotopes are easily fractionally separated from the krypton-85. After ten days to three weeks, the xenon portion of the radioactive gas release reduces to xenon-131m in the presence of fifty times as much, or more, xenon-133.

Xenon-131m and Xenon-133 Decay Data. Xenon-131m is an excited state of stable xenon-131, 163.72 keV above the ground state. It has a 11.8 day half-life and decays principally (98%) through an internal conversion electron with the balance (2%) decaying via gamma ray emission. Its energy spectrum is dominated by internal conversion electrons, characteristic xenon k-shell x-rays and Auger electrons. The decay scheme of xenon-131m is presented in Figure 3.5.

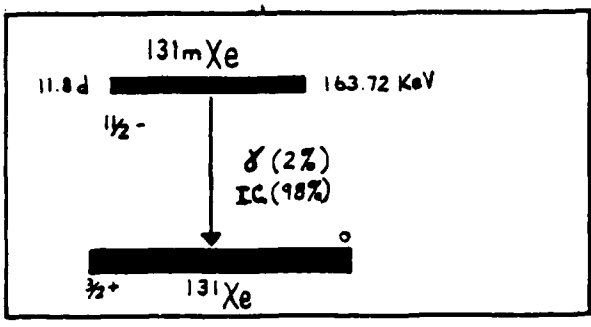

Figure 3.5. Xenon-131m Decay Scheme (38:277)

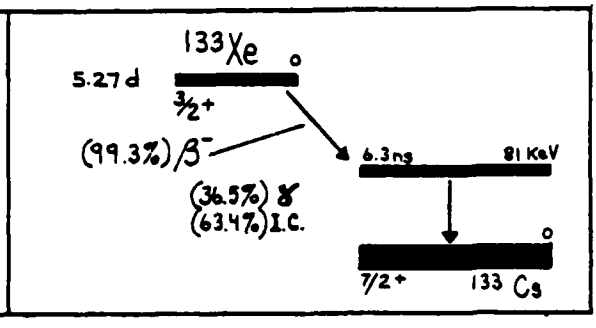

Figure 3.6. Xenon-133 Decay Scheme (38:281)

The decay scheme of xenon-133 is presented at Figure 3.6. Xenon-133 is a radioactive isotope of xenon with a half-life of 5.27 days which decays principally (99.3%) by beta emission to an excited

state of cesium-133, 81 keV above the ground state. This excited cesium-133 decays by internal conversion electron (63.4%) and gamma ray emission (36.5%). The energy spectrum of this xenon radioisotope includes contributions from photo-electrons, internal conversion electrons, cesium x-rays and Auger electrons. Detailed nuclear decay data for xenon-131m and xenon-133 are listed in Table 3.9.

Table 3.9

Characteristic Radiations of ^{131m}Xe and ^{133}Xe

Radiation Type	Energy	Fraction per Decay
^{131m}Xe		
Auger-L	3.43	0.75
Auger-K	24.6	0.068
Ce-K	129.369	0.612
Ce-L	158.477	0.286
Ce-M	162.788	0.0650
Ce-NOP	163.722	0.0178
X-ray-L	4.1	0.080
X-ray $K\alpha_2$	29.458	0.155
X-ray $K\alpha_1$	29.779	0.287
X-ray K_β	33.6	0.102
Gamma	163.722	0.0196
^{133}Xe		
Auger-L	3.55	0.497
Auger-K	25.5	0.056
Ce-K	45.012	0.533
Ce-L	75.283	0.081
Ce-M	79.780	0.016
Ce-NOP	80.766	0.004
β^- Maximum	346.3	0.993
Average	100.6	0.993
X-ray L	4.29	0.061
X-ray $K\alpha_2$	30.625	0.136
X-ray $K\alpha_1$	30.973	0.253
X-ray K_β	35.0	0.091
Gamma	80.997	0.365

(36:138)

Predicted Radioactive Xenon Gas Spectrum

Considering the expected detector resolutions, physical characteristics of the argon fill gas and the nuclear decay data for the two xenon radioisotopes, the high pressure proportional detector's response to a radioactive xenon gas sample can be predicted in the form of a combined pulse height spectrum. Figure 3.7 presents the combined spectrum expected from ^{131m}Xe and ^{133}Xe.

This semi-empirical estimate of the combined spectrum (for 50 atmospheres) required that several assumptions be made. First, total counts for ^{133}Xe (5000 cts) and ^{131m}Xe (100 cts) are assumed, reflecting the expected fifty to one ratio. Second, the most energetic beta particles (346 keV) and conversion electrons (164 keV) are stopped with 85% and 95% efficiency, respectively. Third, less energetic conversion electrons and associated x-rays or Auger electrons are fully stopped or

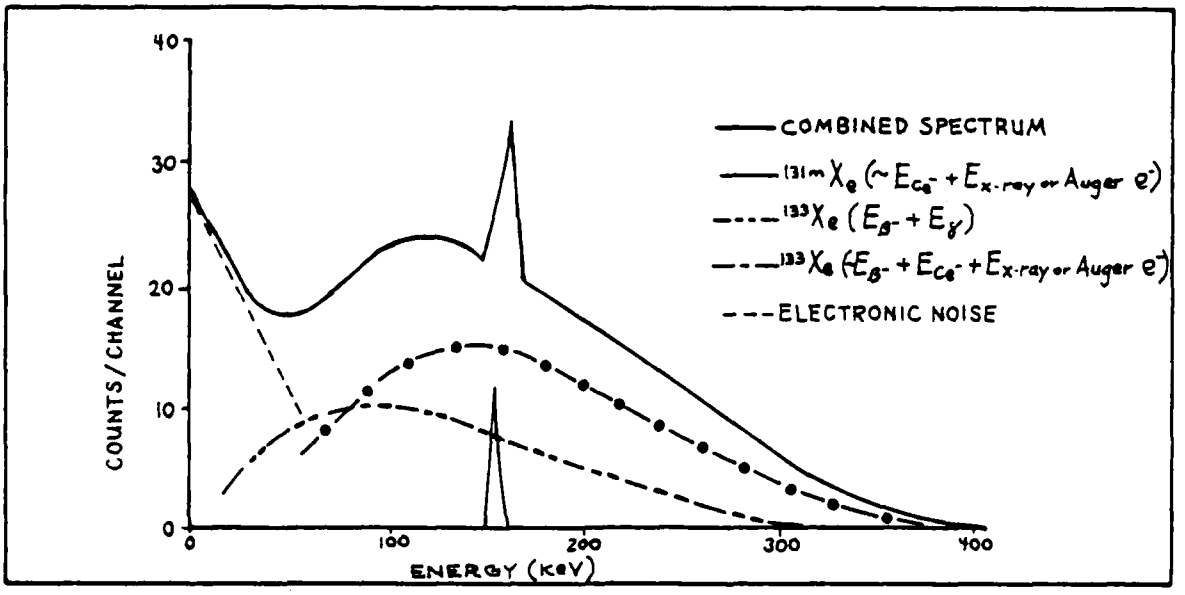

Figure 3.7. Expected Radioactive Xenon Spectrum.

absorbed. Fourth, few (~5%) gammas are fully absorbed in the fill gas. Fifth, the 164 keV sum peak is gausian in shape with a 5 keV fwhm resolution. Finally, background counts are negligible. With these assumptions, the ratio of counts in the 164 keV sum peak (^{131m}Xe) to those in the beta spectrum (^{133}Xe) should allow qualitative and quantitative analysis of the sample.

Achieving these predicted results would demonstrate the ability of the high pressure proportional counter with its associated equipment to analyze noble gas radioisotopes. The full description of this equipment is presented in the following chapter.

IV. Equipment

The detection system has three functional areas. The first general area is the gas handling system which supplies measured quantities of purified counting gas and radioactive gas samples to the detector. The second part of the detection system is the high pressure proportional detector, itself. The third functional area consists of supporting electronics which shape and record the signal from the detector. This chapter provides a detailed description of these subsystems to include specifications for equipment of special design and identification of conventional equipment and apparatus used.

The Gas Handling System

The first part of the detection apparatus is the gas handling system which has four sections. These sections include a conventional fast pumping and vacuum section, a filling and recovery section, a gas purification section with a cryogenic pumping station ("cold finger"), and, a quench gas filling section. These sections allow the detection system as a whole to be evacuated to low vacuum pressures, permit carrier and radioactive sample gases to be fed into the system and provide for purification of the detecting media to remove electronegative impurities. Additionally, a cryogenic pumping point is included to transfer the gases through the purification train, and a feed inlet is included to inject quench gas, which is used to stabilize the multiplication process as previously discussed. Apart from the quartz purification tube, steel gas reservoir cylinder and some vacuum connections, the bulk of the gas handling system is constructed entirely of stainless steel.

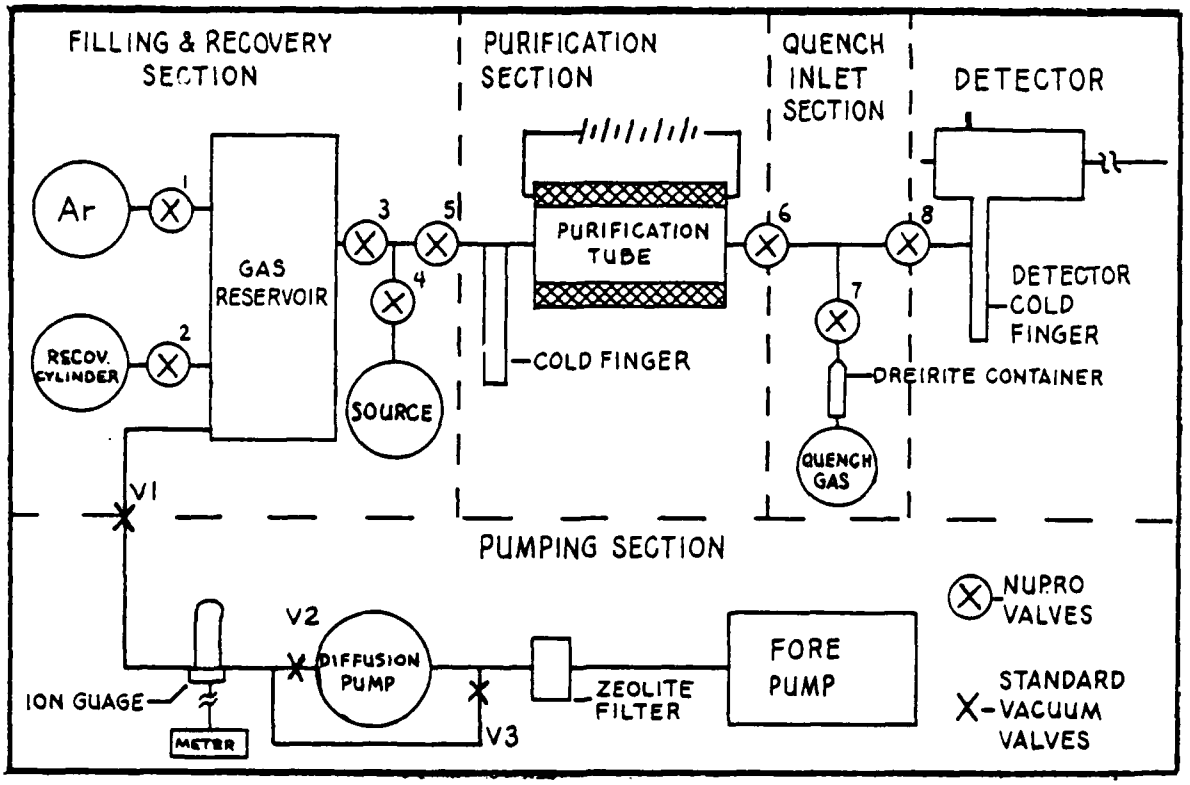

Figure 4.1. Schematic Arrangement of the Gas Handling System

The gas handling system is principally 0.25-inch stainless steel tubing connected either to Nupro control valves with swagelok fittings or connected to Varian knife-edge flanges with copper o-ring seals. Figure 4.1 shows a schematic arrangement of the gas handling system with its various functional areas and sections.

Pumping Section. The fast pumping or vacuum section consists of a forepump and a diffusion pump with a zeolite filter located between them. An ionization vacuum gauge is positioned forward of the diffusion pump and has a range from 10^{-4} torr to 10^{-8} torr. The forepump can reduce the pressure in the filling and recovery section to 10^{-} torr in one to two minutes, while the diffusion pump can be subsequently used to reduce this pressure to below 10^{-6} torr in an additional five

minutes. Standard vacuum valves are used with the bypass connection which segregates the diffusion pump when required. Another standard vacuum valve connects the pumping section to the filling and recovery section and the balance of the gas handling system.

Filling and Recovery Section. The filling and recovery section includes a known volume gas reservoir, a counting gas feed connection, a recovery cylinder connection and a separate feed connection for radioactive gas samples. The gas reservoir is a locally constructed steel container with a volume of 12.34 liters, including tubes connected to three adjacent Nupro valves and the standard vacuum valve. A Pace transducer pressure gauge is located at the top of the gas reservoir and is connected to a Validyne CD23 digital meter. Valve 1 allows the counting gas to enter the system from storage cylinders. Valve 2 connects to a small recovery cylinder which is inserted into a large liquid nitrogen dewar to recover radioactive gas samples or expensive xenon counting gas, when used. Valve "V1" is connected to the pumping section. Finally, the sample inlet, valve 4, is connected to a stainless steel adaptor with o-ring seals to accept break seal tubes. The radioactive xenon gas sample is fed into the detection system through this connection. Valve 5 connects the filling and recovery section to the purification section.

Purification Section. The purification section includes a cryogenic pumping point (cold finger), a double element tubular furnace surrounding a quartz tube filled with purifying material and chromel-alumel leads adjacent to the quartz tube for measuring temperatures with a potentiometer. The stainless steel cryogenic pumping point

is used in conjunction with the detector cold finger to pass the counting gas through the purifier. The electric resistance furnace encases a quartz tube filled with titanium and zirconium turnings at 1000°C and is intended to principally remove oxygen and nitrogen impurities. Chromel-alumel thermocouples are connected to a potentiometer to monitor the temperature. It should be pointed out that though quartz tubing has an approximate softening point of 1665°C, it has a strain point at 1070°C which is extremely close to the furnace operating temperature. Finally, valve 6 is forward of the purification tube and connects to the quench gas feed section.

Quench Gas Inlet Section. The quench gas feed section is located between the purification section and the detector. Valve 7 allows the quench gas to enter the system and be mixed with the purified counting gas. A drierite (calcium sulfate) container is positioned between this valve and the quench gas cylinders for drying the high purity CO_2, CH_4 or other quench gas. The quench gas serves to stabilize the multiplication characteristics of the counting gas during high pressure counting as previously discussed. Finally, valve 8 connects the entire gas handling system to the detector.

The Detector

The proportional detector is essentially a 5.25-inch long, 3.0-inch diameter stainless steel cylinder with 0.69-inch thick walls and 0.625-inch thick stainless steel end caps bolted at both ends. Soft Varian copper gaskets seal the end caps to the case. Internally, an insulator base, a guard tube, a field tube and a support tube are bonded with epoxy to the inner face of the end caps and are insulated with

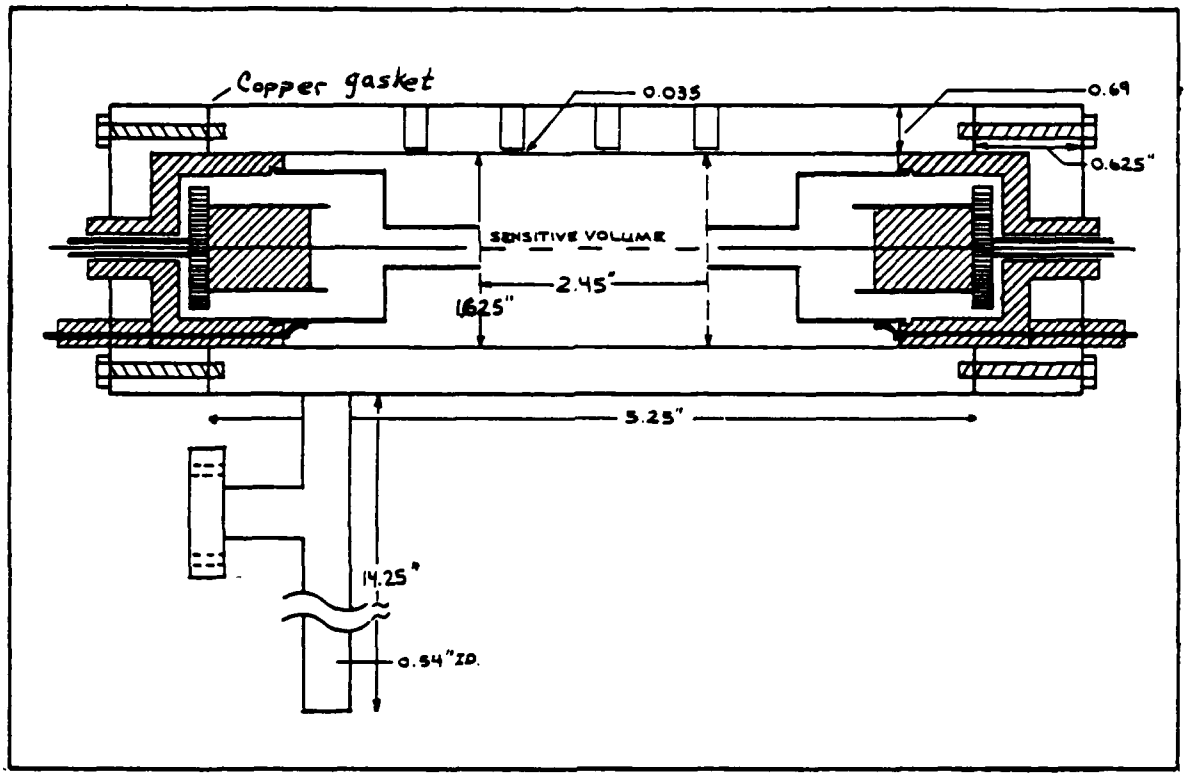

Figure 4.2. The High Pressure Proportional Detector

additional plexiglass fittings. A 0.0003-inch stainless steel anode wire is suspended along the cylinder's axis. Lastly, a stainless steel cold finger, fixed to the bottom of the detector case, has a connection to the gas handling system. A diagram of the proportional detector is shown in Figure 4.2.

Cathode Case and Cold Finger. The external detector components include the cathode case, end caps with copper seals and the attached cold finger with gas inlet connection. The detector case is machined from 304 stainless steel tubing. It is 5.25-inches in length with a 3.0-inch outer diameter and a 0.69-inch wall. Both ends of the cylinder are machined to provide a knife-edge rim for sealing on the Varian

copper gasket to the end caps. A brass plug connector is screwed into the top of the cathode body for the high voltage supply cable connection. Four equally spaced 0.125-inch diameter wells are drilled into the top of the case reducing the cathode wall thickness to approximately 0.035-inches at the base of the wells. These wells allow external low energy gamma sources to be used. The equal spacing permits position dependence of the multiplication process to be investigated.

A vertical 14.75-inch long, 0.54-inch diameter stainless steel tube attached to the base of the detector case forms the cold finger. It is heliarc-welded and (subsequently) silver soldered to an opening, centered 1.0-inch from the edge of the cylinder rim. The cold finger has 0.165-inch thick walls. Horizontal tubing of the same diameter, centered 1.5-inches from the bottom of the case, is similarly attached to the cold finger and connects to the gas handling system.

End Cap Assembly. The stainless steel end caps have plexiglass insulators on their inner face. A guard tube is inserted into a well in the insulator and extends, through a center hole, 0.5-inches beyond the outer face of the end caps. A field tube is fixed to the top rim of the plexiglass insulator well, covers the guard tube, and extends toward the center of the detector. An insulated field tube electrical connection extends through the insulator to the outer face of the end cap. Plexiglass insulators at both ends of the guard tube position the anode wire support tube. This support tube extends outside both ends of the guard tube. The anode wire is inserted into the support tube along the axis of the cylindrical detector. A pin wedged into

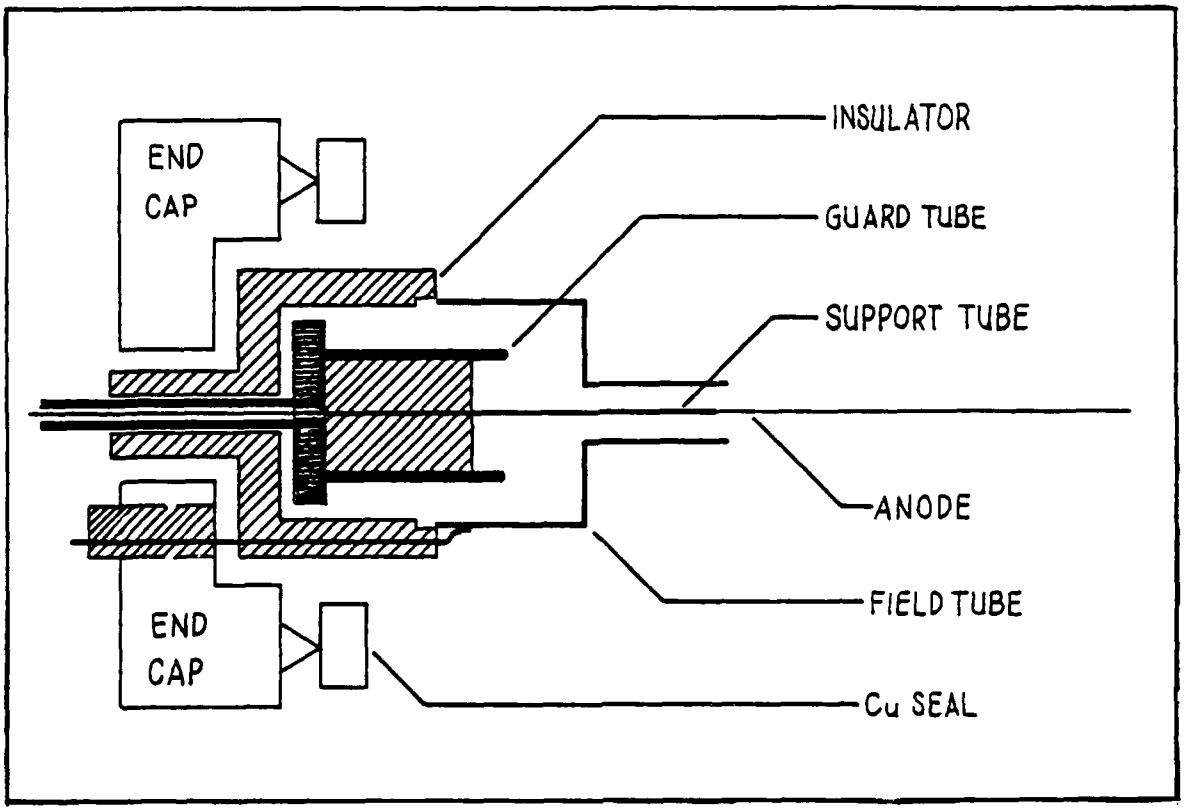

Figure 4.3. Expanded View of End Cap Assembly

the support tube holds the anode wire in place. An electrical connection covers the pin and outer support tube end. Low vapor epoxy is used throughout to bond all components together and to form a vacuum tight seal. Figure 4.3 shows an expanded view of the end cap assembly.

Metal End Cap. The end caps are machined from 0.625-inch thick, 3.0-inch diameter 304 stainless steel disks. A 0.625-inch diameter hole is centered on the outer face with a second, 0.375-inch diameter, hole approximately one inch off center. The inner face of the end cap has a knife-edge rim for sealing against a 2.0-inch diameter copper gasket. The end caps are bolted directly into the ends of the cathode shell with six 0.25-inch diameter, 1.5-inch metal screws. A 1.375-inch

diameter well is machined half way through the inner face of the end caps (0.3125-inches) with the two previously described holes extending through to the outer face.

Insulator Base. A plexiglass cylindrical insulator base is machined to fit in the well of the inner face of the end cap and extend through its center opening flush with the exterior face. A small plexiglass insert fits into the off-centered opening. The plexiglass insulator base extends 0.3125-inches beyond the inner face of the end caps. A 0.75-inch diameter well is drilled into the plexiglass inner face (0.4375-inches deep). A 0.25-inch diameter center hole extends from the base of the insulator well, through the center plexiglass extension to the outer face of the end cap.

Guard Tube. A machined single-piece stainless steel guard tube is inserted into the well of the plexiglass insulator. The guard tube consists of a 0.75-inch diameter, 0.125-inch thick annulus fit into the base of the insulator well with a 0.1-inch center hole. A 0.5-inch diameter, 0.5-inch long tube extends from the annulus out of the well toward the detector's center, and a 0.25-inch diameter, 1.0-inch long tube extends from the annulus at the base of the insulator well to the outer face of the end cap. The external portion of the guard tube extends 0.5-inches beyond the outer face of the end cap.

Field Tube. A machined one-piece stainless steel field tube fits on a circular rim at the top of the well in the plexiglass insulator and covers the inner extension of the guard tube. The 0.75-inch diameter, 0.4-inch long field tube is enclosed at the end facing the detector's center, has a 0.3-inch center hole and a 0.368-inch diameter center tube extending 0.81-inches past the sealed end. An electrical

contact at the wide base of the field tube is connected to a 2.5-inch long metal screw which extends through a hole in the end cap insulator and the insulator in the off-centered hole on the outer face of the end cap. This plexiglass insulated connection previously extended 0.25-inches beyond the end cap face, but was increased to one inch to eliminate electrical discharges previously discussed.

Support Tube. A 0.125-inch diameter, 3.0-inch long anode wire support tube is positioned by two plexiglass inserts at the ends of the guard tube. The external insulator is 0.5-inches long with 0.1875-inch diameter, while the internal insulator is 0.375-inches long with 0.43-inch diameter. Center holes accept the support tubes. The support tube extends slightly past the external portion of the guard tube, extends an inch past the inner portion of the guard tube and is just below the field tube's extension near the detector's center.

Anode Wire. All parts of the end cap assembly are epoxyed together using special low vapor vacuum epoxy. With the assembled end caps bolted to the cathode shell, the 0.0003-inch diameter 304 stainless steel anode wire is inserted through the support tube. With tension applied to the anode wire, 0.25-inch long pins wedge the wire to the outer ends of the support tubes. Solid electrode connections with 0.25-inch deep holes in one end slide over the wedged pins onto the support tubes. Beads of epoxy seal the support tubes and fasten the electrode covers.

Electronics

The charge collected at the anode is converted to a voltage pulse

by an ORTEC 109 PC preamplifier. Signal pulses from the preamplifier are shaped using an ORTEC 572 linear amplifier. These signals are monitored on an oscilloscope and are fed to a Nuclear Data Model 2200 multichannel analyzer. A PERTEC tape recording system is linked to the MCA for spectra storage. A typewriter link provides channel read-out, while a link to a plotter provides graphic support. A single channel analyzer and counter/timer are used to analyze specific portions of the spectra. Figure 4.4 shows a schematic diagram of the detector's supporting electronics.

Finally, two model AEC-5000 NIM standard high voltage power supplies provided power to the cathode and field tubes. Negative polarity was used to allow anode operation at ground potential.

This concludes the description of the electronics used to support the high pressure proportional detector and associated detection system. Operation of this system and various other procedures are covered in the following chapter.

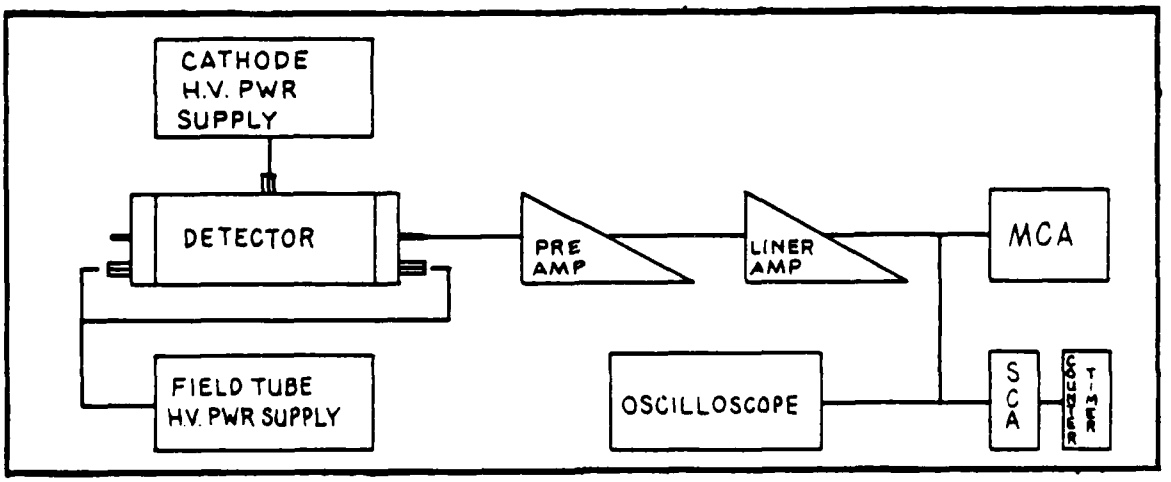

Figure 4.4 Schematic of Detector's Supporting Electronics

V. Procedure

General

The operation of the high pressure proportional detection system involves four separate and sequential procedures. Charging the system is the first procedure. This step involves evacuating the entire system and measuring specific quantities of counting gas into the known volume gas reservoir. The next required procedure is the purification of the counting gas to remove electronegative impurities. The two cold fingers located on opposite ends of the quartz purification tube are used to cryogenically pump the counting gas through the purification train and back again. The third procedure involves introducing the radioactive sources. External gamma ray sources are placed on top of the cathode case over source wells described in the previous chapter. Internally introduced radioactive gas samples are injected into the system at the breakseal tube connection. Collecting data is the last procedure used when operating the detection system.

Charging the System

The first required operating procedure is charging the system with the necessary quantity of counting gas. This four step procedure involves evacuating the system, flushing the system, outgassing the purification material, and injecting the counting gas into the gas reservoir.

Initially, the entire system is evacuated using the forepump and the diffusion pump. This produces a vacuum of 10^{-6} torr, or less. The system is then flushed with 99.999% pure argon. This is

accomplished by charging the system with argon to a pressure of 100 mmHg. By-passing the diffusion pump, the forepump evacuates the system to 25 μmHg. Then the diffusion pump is used to evacuate the system to below 10^{-6} torr. This process is repeated four times.

After flushing the system, the purification material is heated to 1000°C. This material is then allowed to outgas overnight while the pumping section maintains the vacuum at or below 10^{-6} torr. Subsequently, the argon counting gas is fed into the known volume gas reservoir. Pressure readings from the gas reservoir allow the injection of precise amounts of the counting gas. Van der Waal's equation is used to calculate the quantity required to produce the high pressure desired in the detector volume.

Purifying the Counting Gas

After charging the system, the counting gas must be purified to remove impurities. First, the gas is allowed to expand into the remainder of the detection system. A dewar of liquid nitrogen is slowly raised around the detector's cold finger. The valve adjacent to the quartz purification train is used to regulate the flow of the gas. The bulk of the counting gas passes through the zirconium and titanium turnings (at 1000°C) inside the purification tube. After the gas condenses and solidifies in the detector cold finger, the valve which separates the gas reservoir from the remainder of the system is closed. Allowance is made for argon vapor which is not solidified and remains in the reservoir.

The counting gas is then passed back through the purification train by slowly lowering the dewar at the detector cold finger, while a second dewar of liquid nitrogen is slowly raised around the cold

finger adjacent to the purification tube. Each pass between cold fingers requires sixty to ninety minutes. Caution must be exercised after closing the valve to the reservoir. If the condensed argon is allowed to completely vaporize within the detector and purification train volumes, the pressure would cause the quartz tubing to burst. Normally the procedure is repeated through four cycles and requires ten to twelve hours to complete the purification process. With the purified counting gas condensed inside the detector cold finger, the valve adjacent to the detector is closed. Again, allowance is made for vapor losses which remain in the purification train. When the counting gas is allowed to vaporize in the detector volume, it develops the required high pressure.

Introducing the Radioactive Sources

With the counting gas inside the detector, sources are introduced in two ways. External gamma sources are placed over the source wells drilled into the top of the cathode case. Alternately, internal gas sources are introduced at the breakseal tube connection, cryogenically pumped into the detector and mixed with the counting gas.

External Gamma Sources. The encased gamma sources are fixed to plexiglass discs with center extensions on the bottom which fit into the source wells at the top of the cathode case. The base of the well is approximately 0.035-inches thick as described in Chapter IV. Plexiglass tongs are used to place the different sources directly on the cathode when operating voltages are applied.

Internal Sources. Radioactive xenon gas in a breakseal tube is fitted to the gas handling system at the gas source connection.

The valve forward of this connection is closed. The connection tubing is evacuated and purged in the same manner as previously described. The breakseal is broken allowing the radioactive gas to expand into the isolated and evacuated connection. The valve forward of the connection is opened. The radioactive xenon gas is cryogenically pumped through the purification section to the detector cold finger using the dewar of liquid nitrogen, as before. The xenon gas condenses and solidifies in the detector cold finger. Since the vapor pressure of solid xenon at the temperature of boiling liquid nitrogen is~10^{-3} torr (27:800), nearly all of the source is collected in the detector cold finger. The valve adjacent to the detector is closed after allowing sufficient time for the source to be transported to the detector. The counting gas and radioactive xenon source are allowed to expand inside the detector volume.

The Collection of Data

After the counting gas expands inside the detector and the sources are appropriately introduced, data may be collected. Initially, the remainder of the system is evacuated. This is essential to prevent electrical discharges between the negatively biased cathode and the gas handling system which is at ground potential. The quartz insulator tubing which connects the gas handling system to the detector valve assists in this task. The cathode and field tubes are set at their required negative potentials. This polarity allows the anode to be operated at ground potential. Adjustments to the gain and shaping times are made using an oscilloscope to obtain acceptable signals. The signal is then routed to the multi-channel analyzer. A tape recording arrangement allows recorded spectra to be permanently stored.

VI. Results

This research continued Knapp's study (34) of the high pressure proportional detection system described in Chapter IV. The detector's operating characteristics and signal resolutions at high pressures are evaluated, based on the theory and reference information described in Chapters II and III, respectively. Characterizing the detector's response was ultimately intended to provide the basis for the qualitative and quantitative analysis of a radioactive noble gas sample.

The approach taken to investigate the detector's response was to organize the research into three general areas. Initially, general research was conducted to correct previously observed faults of the detection system and to calibrate the supporting electronic equipment. Next, the detector's response to several external sources was characterized using argon counting gas at twenty and fifty atmospheres. The last research efforts focused on the analysis of the radioactive xenon gas test sample to demonstrate the utility of the detection system to perform its intended function.

The investigation focused upon five specific facets of the detector's response (for specific gain and bias settings using argon gas at 20 and 50 atmospheres):

1. Energy calibration of the detector (MCA channel numbers versus radiation energy)
2. Multiplication factors for the detector (multiplication factor versus cathode bias)
3. Intrinsic efficiencies for external and internal sources (observed counts versus radioactive emissions theoretically entering the detector's sensitive volume)
4. Detector resolutions for specific radiations, energies

and fill gas pressures (log resolution versus log deposited energy); and, optimum spectra resolution for specific gas pressures (resolution versus cathode bias)

5. The effects of impurities, and the need for quench gas (qualitative investigation, rather than a detailed quantitative analysis).

This chapter describes the results which are intended to characterize the detector's response. The presentation of results parallels the organization of the research, itself. General calibration results are presented first. Results obtained using external sources at both twenty and fifty atmospheres are then described. Last, the results of the radioactive xenon noble gas sample analysis are presented.

General Calibration Results

Preliminary research was conducted to resolve limitations associated with detector's operating range and to calibrate the gas handling system and the supporting electronic equipment.

Results of Detector Modifications. Knapp described discharges at the external field tube connector (34:79), and secondly, between the guard tube and cathode (34:71). These discharges limited the maximum cathode voltage which could be applied. In turn, this limited the size of the multiplication process. To correct these problems a covered extension was added to the external connector and epoxy was applied to likely discharge points inside the detector. These discharges were eliminated as a result.

A second modification to the detector included installation of a smaller, 0.3-mil anode wire (0.0003-inch diameter). Previously, 0.4- and 0.5-mil wires had been used. The smaller diameter would reduce the required operating voltages as seen from the Diethorn

relation, equation (2.20). Table 6.1 compares the cathode bias necessary to obtain multiplication factors of one and ten when each wire is installed in the detector.

Table 6.1

Cathode Bias for Different Anode Wire Diameters

	CATHODE VOLTAGES (V)*			
Anode	20 Atmospheres		50 Atmospheres	
Diameter (mil)	M = 1.0	M = 10.0	M = 1.0	M = 10.0
0.3	960	1600	2400	3125
0.4	1250	1875	3100	3800
0.5	1525	2150	3775	4475

(*Argon Diethorn constants used: $\Delta v \simeq 28$ eV, $k \simeq 1.45 \times 10^4$ V/cm-atm; b = 2.064 cm)

These lowered voltage requirements also allowed the use of more stable high power sources which Knapp was not able to utilize for the upper limits of the operating range (M ≃ 100).

Four source wells were installed as the last modification to the detector to allow external gamma or x-ray sources to be used for calibration purposes. The wells were drilled on 0.75-inch centers beginning at the end of the field tube. Figure 4.2 indicates the approximate positions. Figure 6.1 illustrates the actual dimensions and the

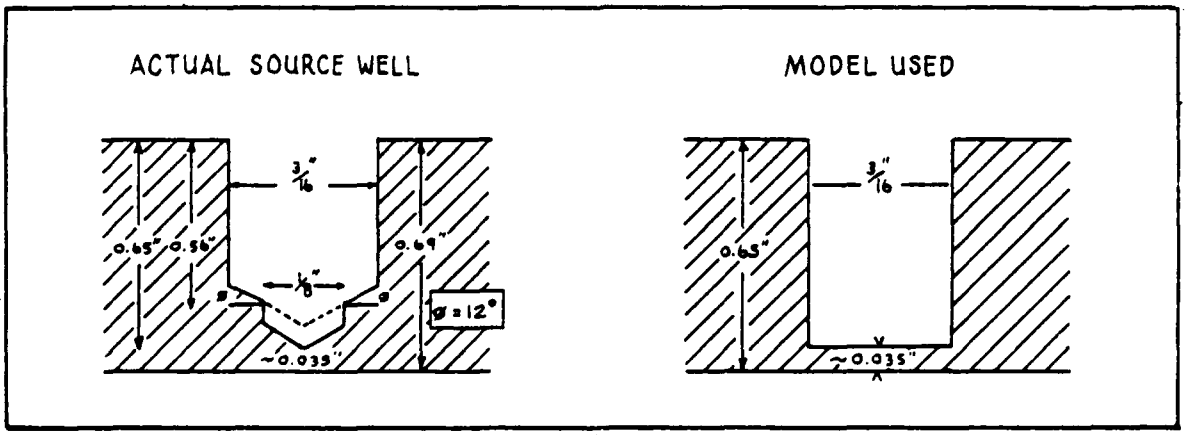

Figure 6.1. Construction of Source Wells

simplified model used to later calculate geometric factors and absorption/scattering factors.

Results of Equipment Calibration. Following the modifications to the detector itself, the gas handling system, the preamplifier and multichannel analyzer were calibrated.

Volumes. The critical volumes included the gas reservoir (12.340 liters) and the detector (0.197 liters). The remainder of the gas handling system between the reservoir and detector was 0.175 liters. The volumes for each subsection of the gas handling system are fully specified in Appendix A.

Preamplifier. Calibrating the electronic equipment was necessary to evaluate the output signal pulses. The final pulse height measured (in millivolts) is the result of several contributions and is given by

$$ph = (No \cdot e) \cdot (G_Q G_V)_{PA} \cdot (G_{LA}) \cdot M(V) \qquad (6.1)$$

where

$(No \cdot e)$ = total charge of the primary ion pairs [pC]

$(G_Q)_{PA}$ = preamp voltage pulse to charge gain [mV/pC]

$(G_V)_{PA}$ = preamp voltage gain [dimensionless]

G_{LA} = Linear amplifier voltage gain [dimensionless]

$M(V)$ = Multiplication factor for specified cathode bias [dimensionless]

Normally, equation (6.1) is modified by introducing equation (2.11), which gives

$$ph = (E_{dep} \cdot e/W) \cdot (G_Q G_V)_{PA} \cdot (G_{LA}) \cdot M(V) \qquad (6.2)$$

The calibration information available for the preamplifier did not directly specify the pulse to charge gain (G_{Q-PA}). Rather, the pulse for a MeV deposited in silicon (W_{Si} = 3.62 eV/ip) was reported to produce a twenty millivolt pulse, or

$$(e / W_{Si}) \cdot (G_Q)_{PA} = 20 \text{ mV/MeV} \tag{6.3}$$

Likewise, the corresponding value for argon (W_{ar} = 26.2 eV/ip) would be

$$(e / W_{ar}) \cdot (G_Q)_{PA} = \frac{(20)\ (3.62)}{(26.2)} \text{ mV/MeV} \tag{6.4}$$

$$\simeq 2.76 \text{ mV/MeV}$$

Table 6.2 lists the voltage pulses expected for various energies deposited in argon fill gas. These pulses could be correlated to the sources listed, assuming all quanta are stopped in the detector's sensitive volume and all energy is fully deposited.

Table 6.2

Expected Pulses in Argon

E_{dep} [keV]	$(E_{dep} \cdot e / W_{AR}) \cdot (G_Q)_{PA}$ [mV] *	Sources
60	0.166	^{241}Am (γ)
88	0.243	^{109}Cd (γ)
100.6	0.278	^{133}Xe (β^-avg)
122	0.337	^{57}Co (γ)
164	0.453	^{131m}Xe (C_{e^-})
346	0.956	^{133}Xe (β^-max)

* Given: $G_{v-pa} = G_{LA} = M(v) = 10.0$

The preamplifier is calibrated to produce two thousand two hundred and ninety ion pairs for 60 keV deposited in argon, with the total charge correlated to a 0.166 volt pulse (where $G_{V-PA} = G_{LA} = M(v) = 10.0$).

MCA. The signal is transmitted to the multichannel pulse height analyzer. Various channels (1024 in this case) can be calibrated such that counts recorded at specific channel numbers (CN_{MCA}) correspond to specific voltages. A pulser was used to calibrate the MCA and produced the following linear regression correlation

$$ph = B_{MCA} \cdot CN_{MCA} + A_{MCA} \tag{6.5}$$

where

$B_{MCA} = 9.182152$ [mV/cn]

$A_{MCA} = -85.59767$ [mV]

Results of Background Counting. A final preliminary investigation included measuring background counts using the detector without introducing radioactive sources. Background counts averaged approximately 0.01 counts per channel per second. This value was negligible in comparison to source counting rates (essentially three to four orders of magnitude apart).

With the detector modifications accomplished, calibration completed and background counts evaluated, the second phase of the research was begun.

Results Using External Sources

The research with external sources was intended to characterize the detector's response at twenty and fifty atmospheres. In part,

determining the multiplication factors at specific voltages, calculating the intrinsic efficiencies and measuring the spectra resolutions allowed the detector to be calibrated and operated under optimum conditions. Auxiliary areas were qualitatively investigated, time and success in other areas permitting.

Multiplication Factors. The calibration data from the preamplifier and MCA allowed the multiplication factors to be calculated directly using equations (6.2) and (6.4). However, the detector pressure was not measured directly. Rather, fill gas was cryogenically condensed in the detector from the known volume and pressure in the gas reservoir. As described in Chapter V, van der Waal's equation was then used to calculate the detector's pressure.

The lengthy purification process encouraged efficient (multiple) use of the purified fill gas. Thus, the lower pressure data was obtained by cryogenically condensing the fill gas (at 50 atmospheres) in the detector cold finger and carefully back venting gas into the gas reservoir until predetermined pressures in the reservoir were obtained. Again, direct measurement was not accomplished.

This approach required assuming that the gas in the detector was constant or at least known. Though the end caps were bolted with sufficient torque to require frequent replacement of the bolts, leak rates were significant and varied for different data collection runs. For example, the loss rate for run 6 averaged approximately 0.079 atmospheres per hour (~1.9 atm./day). Gas purification required twelve to fourteen hours, and data collection for a single gas pressure typically involved six to eight hours. The pressure could vary nearly two atmospheres during a single run.

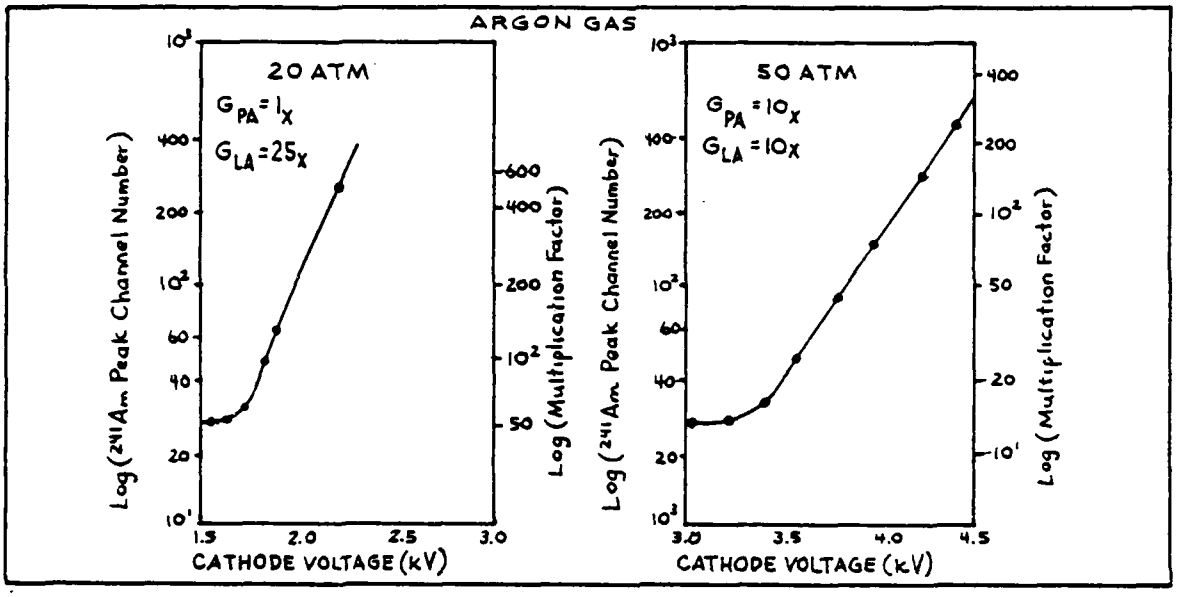

Figure 6.2. Experimental Argon Gas Multiplication Curves.

Additionally, gas purity varied among the various runs in a manner which was only qualitatively characterized. This topic is discussed further in a separate subsection of this chapter. With these limitations in mind, typical multiplication factors measured for two pressures are graphically depicted at Figure 6.2, and are listed at Table 6.3.

Table 6.3

Typical Experimental Argon Gas Multiplication Data

20 Atmospheres[a]			50 Atmospheres[b]		
Cathode Bias (V)	MCA CN	Calculated Mult. Factors	Cathode Bias (V)	MCA CN	Calculated Mult. Factors
-	-	-	3200	27	10.2
-	-	-	3400	35	14.7
-	-	-	3600	51	23.9
1700	30	47.5	3800	91	46.9
1800	51	93.4	4000	143	76.7
1860	65	128	4200	297	~140
1920	89	~183	-	-	-

([a]: G_{V-PA} = 1x, G_{LA} = 25x; [b]: G_{V-PA} = 10x, G_{LA} = 10x)

These multiplication factors can be approximated using rough Diethorn constants estimated from the data (for $1.0 \leq M \leq 10$). However, more accurate correlations to calculate these factors were obtained for each (separate) pressure using simple linear regression formulas. These equations are accurate (~3% error) over the range of interest and have the following form

$$M_p(V) = \exp (B_p \cdot V + A_p) \qquad (6.6)$$

where

$M_p(V)$ = the multiplication factor for the specific voltage and pressure, P (20 and 50 atmospheres, only)

B_p, A_p = calculated constants for the specific fill gas pressure

The estimated Diethorn constants, used with equation (2.20) and the calculated single pressure data fit constants, used with equation (6.6) are listed at Table 6.4.

Table 6.4

Experimental Argon Gas Multiplication Factor Constants

	Linear Regression Constants		Diethorn Constants	
Pressure (ATM)	A_p	$B_p(V^{-1})$	Δv(ev)	k(V/cm-atm)
25	-5.55910	5.60496×10^{-3}	~28	$\sim 1.45 \times 10^{4}$
50	-6.07695	2.5976×10^{-3}	~28	$\sim 1.45 \times 10^{4}$

Diethorn constants for numerous mixtures of noble gases are available in the literature (35:195), but not for pure argon or xenon.

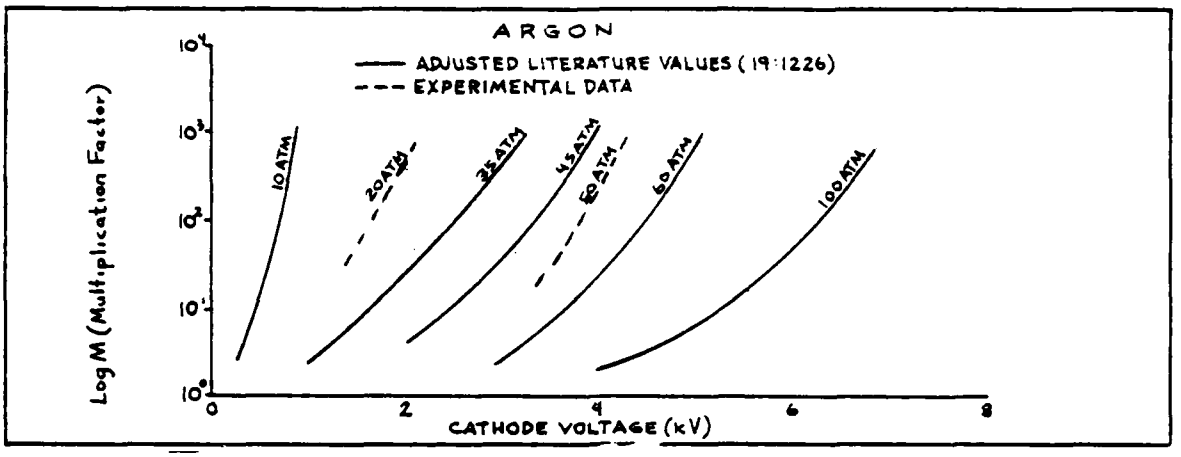

Figure 6.3. Experimental Multiplication Curves Compared to Reconstructed Literature (19:1226) Curves.

However, the data from Figure 2.3 (19:1226) was modified to approximate curves expected if local detector dimensions had been utilized (a = 3.81 μm, b = 20.64 mm), rather than those cited in the reference (a = 20 μm, 6 = 6 mm). This comparison of results is presented at Figure 6.3.

Energy Calibration. After determining multiplication factors as a function of the cathode bias, equations (6.1), (6.4) and (6.5) readily permitted the calibration of the detector, as below

$$E_{dep}\ [MeV] = \frac{(B_{MCA}\ CN_{MCA} + A_{MCA})}{20 \cdot (3.62/26.2) \cdot G_{V-PA} \cdot G_{LA} \cdot M(v)} \qquad (6.7)$$

From the fifty-atmosphere data and cathode bias set at 4.0 kV, channel number 143 was recorded for the 60 keV ^{241}Am photopeak. When the appropriate gains and multiplication factor (G_{V-PA} = 10x, G_{LA} = 10x, M(4.0 kV) = 76.7) are substituted, equation (6.7) yields a 58 keV value (~3% error) for the energy deposited. Using the regression data fit constants, the multiplication factor obtained was 74.7 (~3% error).

When substituted into equation (6.7) along with the experimental settings, the energy deposited was estimated 59.55 keV (~0% error).

Intrinsic Efficiency. The intrinsic efficiency must be known to fully calibrate the detector. The task is accomplished by totaling the counts recorded under a specific energy peak and comparing that total to the number of quanta which enter the detector's sensitive volume during the counting time. The total of the specific quanta theoretically emitted is calculated using equations (2.2) and (2.3). The source activity is reduced by the branching ratio for the quanta of interest. These counts are further reduced by spherical divergence, absorptions from intervening material and by quanta which enter the detector's sensitive volume but ultimately escape undetected. The calculation of these factors and the resulting intrinsic efficiencies for each source and pressure used are described in the following subsections. The results of these calculations are listed in Table 6.5. Appendix B provides specific sample calculations, along with the necessary reference values used.

Geometric Factors. The external gamma sources are placed directly over the source wells, are modelled as point sources and are reduced by spherical divergence. This divergence is defined by the source well model dimensions illustrated in Figure 6.1. Equation (2.5) is used to calculate these factors. The specific result is presented below. The calculation of this value is presented in Appendix B.

$$f_g \approx 5.12 \times 10^{-3} \tag{6.8}$$

Transmission Factors. The reduction factors for intervening material is calculated using equation (2.6) for the 0.035-inch stainless

steel source well base. Though 304 stainless is an alloy (~68.7% Fe, ~19% Cr, ~9% Ni, ~2% Mn, ~1% Si and ≤ .08% C), total cross sections (40) for iron are used to simplify the necessary number of calculations. The external photons are attenuated by a factor of 44%, 71% and 82% for 60 keV, 88 keV and 122 keV photons, respectively. Sample calculations are included in Appendix B.

Photon Escape Factors. Equation 2.7 is used to calculate the fraction of photons which enter the detector's sensitive volume and are absorbed (detected) by the counting gas. The remainder escape. Photoelectric and Compton-scatter cross sections are obtained from references (40). Necessary gas densities are calculated using van der Waal's equation (ratio of gram atomic weight and VDW gas volume). The distance traveled by the photons through the fill gas is taken as the diameter of the detector. The fraction of photons (60-122 keV) in the counting gas ranged 5.4 - 2.2% (at 20 atmospheres) and 13.4 - 55% (at 50 atmospheres). A complete listing is at Table 6.5. Detailed calculations are at Appendix B.

Electron Escape Factors. The photons which are absorbed or scattered in the counting gas impart their energy to single electrons during each interaction. The fraction of these energetic electrons which are stopped in the sensitive volume of the detector is calculated using equation (2.9). The remaining fraction is absorbed by the detector's inner surfaces. The fraction stopped in the counting gas ranged from 92 - 81% (at 20 atmospheres) and from 97 - 91% (at 50 atmospheres) for 60 keV and 122 keV electrons (ignoring binding energy), respectively. Table 6.5 presents the complete listing, and Appendix B includes sample calculations.

Intrinsic Efficiencies Calculated. The intrinsic efficiencies are calculated using the total number of interactions experimentally counted in the appropriate photopeak divided by the current theoretical gamma counts of interest (over the counting time), as reduced by the factors already presented. The calculated efficiencies ranged from 17 - 55% (at 20 atmospheres) to 23 - 65% (at 50 atmospheres) for 60 keV and the combined 122/136 keV photopeaks, respectively. A summary of specific gamma activities, all reduction factors calculated and resulting theoretical count rates, are at Table 6.5. Experimental count rates (measured photopeak counts/counting time) and resulting intrinsic efficiencies are also included.

Table 6.5

Intrinsic Efficiencies and Related Factors

Gamma	^{241}Am (60 keV-γ)	^{109}Cd (88 keV γ)	^{57}Co (122+136 keV-γs)
Activity (γs/sec)	15.67×10^4	8.081×10^4	9.070×10^4
fg[a]	5.12×10^{-3}	5.12×10^{-3}	5.12×10^{-3}
f_t[b]	0.440	0.708	0.817
Twenty Atmospheres			
fs_γ[c]	0.054	0.029	0.022
fs_{e-}[d]	0.922	0.868	0.809
Count Rates (Cps)			
Experimental	2.95	2.09	3.71
Theoretical	353.	293.	379.
INTRINSIC EFFICIENCY	0.84%	0.71%	0.98%
Fifty Atmospheres			
fs_γ[c]	0.134	0.074	0.055
fs_{e-}[d]	0.967	0.941	0.905
Count Rates (Cps)			
Experimental	10.45	6.12	12.29
Theoretical	353.	293.	379.
INTRINSIC EFFICIENCY	2.96%	2.09%	3.24%

[a] The geometric factor, fg, is defined on page 82; [b] The transmission factor through the detector wall, f_t, is defined on page 82; [c] The fraction of photons not escaping the sensitive volume, fs_γ, is defined on page 83; [d] The fraction of electrons stopped in the sensitive volume, fs_{e-}, is defined on page 83.

Different data runs exhibited a modest range of efficiencies during the final data runs for the three external sources. However, an interesting fact is that early data runs were fifty percent more efficient. The change is directly related to the inadvertant detector contamination (with dysprosiun) and the subsequently performed cleaning processes (repeated several times) required to return the detector to an acceptable level of operation. A comparison of these early and later intrinsic efficiencies is presented in Table 6.6.

Table 6.6

Comparison of Intrinsic Efficiencies (by Data Run)

Source	Run #7[a] (50 ATM)	Run #9 (50 ATM)	Run #9 (20 ATM)	Run #10 (50 ATM)	Runs 9-10 AVG.
^{241}Am	29.6%	22.9%	16.8%	21.5%	20.4%
^{109}Cd	45.3%	30.0%	28.3%	36.4%	31.6%
^{57}Co	95.1%	65.1%	54.9%	71.5%	63.8%

[a] Last Run Prior to Contamination and Repeated Cleaning Processes.

The contamination problem directly correlated to the loss of effective operation and coincided with the subsequent loss of efficiency. However, a second problem occasionally occurred during this same time frame, which also related to the efficiency calculations. Periodically, counts registered on the MCA were observed to be far fewer than those recorded by a separate SCA/Timer. Improperly positioned MCA toggle switches were frequently found to be the source of this problem. Subsequently, comparisons were made to prevent the second problem from influencing the data collected.

Signal Resolution. As described in the theoretical discussion in Chapter II, the resolution of the output signal is a measure of the detector's ability to detect details in spectra. Resolution is defined in terms of its full width at half the maximum pulse height (fwhm) in equation (2.35). This fwhm is specified in energy units (eg. keV). A common alternate form is obtained by dividing equation (2.35) by the energy deposited to obtain resolution as a fraction of that energy (eg. %). Equation 6.9 presents this alternate formulation

$$\text{Resolution [\%]} = R\ [\%] = 2.36\ [(F + b)\ W/E_{dep}] \qquad (6.9)$$

Evaluation of this equation using the Fano factor (F), avalanche variance (b), and the W-value for 5.9 keV energy deposition in argon results in the limiting resolution (12.8%) from the literature which is presented at Table 2.1. Likewise, the signals produced by the three external gamma sources used in this research have limiting resolutions. Furthermore, where sufficient resolution data is obtained using multiple sources of similar activities and different energies under specific operating conditions, the experimental value for the combined value of the Fano and avalanche variance factors can be calculated as shown in equation (6.10) below.

$$\log R = (\log 2.36 + 0.5 \log [(F + b)\ W\ ]\ ) - 0.5 \log(E_{dep}) \qquad (6.10)$$

where

$$\text{slope} = -0.5$$

$$\text{intercept} = (\log 2.36 + 0.5 \log [(F + b)\ W]\ )$$

The data taken at several pressures and voltages results in various resolutions for different operating conditions. Thus, optimum

operating settings can be identified and used to enhance the results obtained later when utilizing the calibrated detector.

Limiting Resolutions. Where values for F, b and W are substituted into equation (6.9), limiting resolutions for the sources used in this study can be calculated. These values are listed at Table 6.7.

Table 6.7

Limiting Theoretical Resolutions

Source	Gamma(keV)	F	b	W(ev)	Limiting Theoretical Resolution
^{241}Am	59.54	0.17	0.50	26.2	4.05%
^{109}Cd	88.03	0.17	0.50	26.2	3.33%
^{57}Co	122.01	0.17	0.50	26.2	2.83%

Table 6.8 lists typical resolutions obtained for several voltages (and multiplication factors) at 20 and 50 atmospheres. The experimental results have resolutions which are three times the limiting values predicted (on the average).

Table 6.8

Experimental Energy Resolutions

Pressure [ATM]	Mult. Factor	Voltage [V]	Resolutions [% (keV)]		
			^{241}Am	^{109}Cd	^{57}Co
50	14.7	3400	9.4%(5.59)	7.4%(6.52)	9.2%(11.17)
	23.9	3600	7.5%(4.45)	8.8%(7.79)	9.1%(11.13)
	46.9	3800	13.7%(8.15)	11.6%(10.19)	10.4%(12.74)
20	93.4	1800	6.8%(4.05)	7.90%(6.94)	9.0%(10.99)
	128	1860	8.0%(4.74)	8.5%(7.50)	10.4%(12.64)
	~ 183	1920	8.1%(4.80)	8.9%(7.80)	10.3%(12.60)

Furthermore, the ratios of the limiting resolutions expected for different quanta energies for the same detector and operating conditions can be derived from equation (6.9), as given below

$$R_1 = (E_{1\text{-dep}} / E_{2\text{-dep}})^{0.5} \cdot R_2 \qquad (6.11)$$

Evaluation of this equation for ^{241}Am, ^{109}Cd and ^{57}Co results in 1: 0.82: 0.70 ratios for their respective resolutions. The data presented in Table 6.8 does not correlate well with the expected slope given with equation (6.10). Also, the ratios presented above are not observed.

The ^{57}Co source is expected to have poorer resolution than predicted because the 122 keV gamma's photopeak and the 136 keV gamma's photopeak overlap. A resolution of 7 keV would be required to distinguish these two photopeaks. Since the experimental fwhm is on the order of 11-13 keV, counts for these two gammas appear as a single peak. Since the branching ratio for the 122 keV gamma is eight times greater than that of the 136 keV gamma, the resultant peak is centered on the channel associated with the 122 keV energy.

The remaining ^{241}Am and ^{109}Cd photopeaks should follow the predicted slope. The data from the 50-atmosphere pressure run at 3400 volts does approximate the expected proportion (1: 0.82) for signal resolutions. However, several pairs of data presented in Table 6.8 increase with energy, giving a positive slope. From Table 6.5 the theoretical count rate predicted for ^{241}Am is nearly twice that predicted for ^{109}Cd. Statistical considerations may be responsible for this improvement in theoretical and observed resolutions for ^{241}Am.

Further, since the resolution data in Table 6.8 basically includes only two usable data points per operating condition, other

additional data is not available to confirm the experimental slopes derived from the first two data points. The variance in the slopes did not consistently confirm the correct direction (+ or -) of the slope.

Likewise, the resolution data was not consistent enough to support further analysis to calculate the experimental values for the 'F + b' term of the slope listed in equation (6.10).

However, data taken before the detector was contaminated (Run 7) had somewhat poorer resolution values (a result of limited purification of the gas), but consistently had the form predicted in equation (6.10). This data is presented in Table 6.9.

Table 6.9

Precontamination Resolutions

50 ATM Mult. Factor	Voltage (V)	Resolutions (%) ^{241}Am	^{109}Cd	^{57}Co
48.8	3850	18.2	13.1	-
35.4	3700	21.2	17.6	-
21.3	3500	29.9	23.6	-
AVERAGE		23.1	18.1	-

The average slope (-0.637) and the average intercept (+5.542) defined by this data predicted an 'F + b' term 666 times the theoretical value (+0.67), where noise considerations are ignored. This would result in resolutions many times greater than theoretically predicted.

Finally, fwhm associated with noise in the electronics was determined by measuring the resolutions of the signals from the pulser used to calibrate the MCA. For signals stored in channels 0-300 (as in the

case for all data collected in this research), the noise was characterized by a two channel fwhm and represents different energies in accordance with the calibration curve previously presented. The actual equation for the noise is presented in equation (6.12) below

$$\Delta CN_{NOISE}/2 = 1.682 \times 10^{-3} \cdot CN_{MCA}(Peak) + 1.885 \qquad (6.12)$$

Optimum Resolution. The resolutions for the pressures and voltages listed in Table 6.8 did vary. However, because of the trend observed in the data, the optimum operating conditions could not be determined. The best resolution observed for 50 atmospheres of pressure was with 3400-volt cathode bias and gains of ten for both the preamplifier and the linear amplifier (M ≈ 24). Sample spectra for various pressures and voltages (multiplication factors) are presented in Appendix C. See Figure 6.4 for the graphical depiction of the resolution data (resolution vs. cathode voltage).

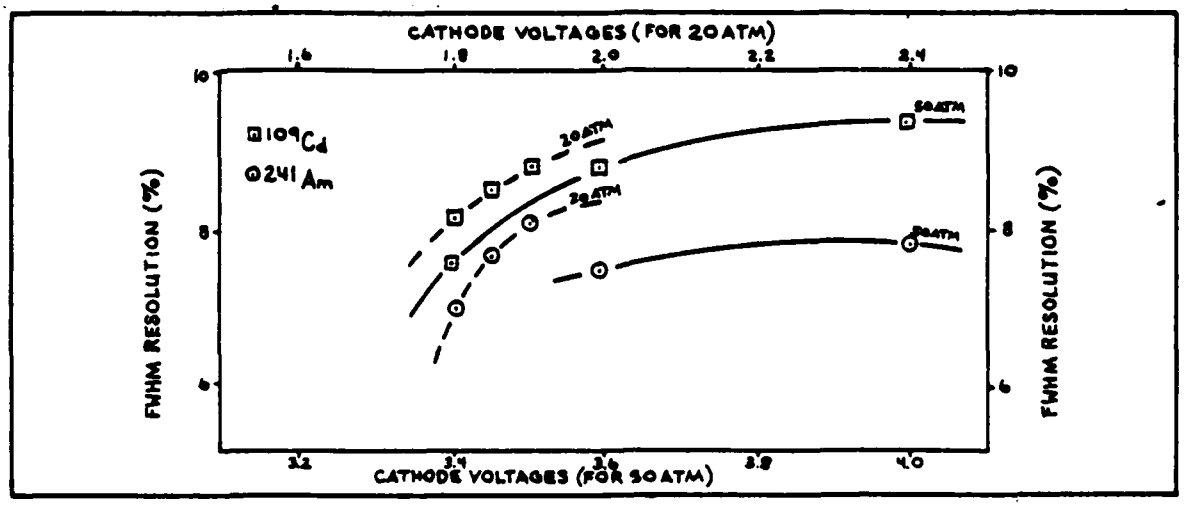

Figure 6.4. Resolution

The Effects of Impurities and the Need for Quench Gas. The problems associated with impurities in the fill gas and the need for quench gas were addressed in this research only in a qualitative manner. Specific data was not collected to properly delineate these considerations. However, the following general observations are presented which indicate certain trends.

Impurities. The level of impurities definitely affected the operation of the high pressure proportional detector as predicted by theory. First, signals were not possible at 50 atmospheres unless the fill gas was first purified. Secondly, resolutions for Run 9 (where the fill gas was transported twelve times through the purification train) were approximately fifty percent better than for Run 7 (where only eight passes through the purification train were completed). No data on flow rates is available as the equipment is presently configured. Finally, in those instances where the same gas was utilized in the detector over a period of several days, impurities associated with leaks and internal gas releases (adsorbed on the detector's inner surfaces) caused the signal to be significantly degraded. Ultimately, this resulted in continuous discharges in the detector rather than in acceptable signals.

Quench Gas. Spurious pulses developed at the higher voltages (where $M \simeq 100$). Initial data was generally taken using a cathode bias approximately 50 volts below this point. In those instances where the detector was operated beyond this point, continuous discharges developed. Frequently the anode wire was destroyed as a consequence of these discharges. Where higher multiplication values are desired, the addition of quench gases and/or Pennings mixtures is obviously

needed, as predicted by theory and suggested in this research. Questions regarding proper methods for purifying the fill gases after the addition of a quench gas are unresolved.

Other Considerations. Source wells distributed along the length of the anode wire permit investigation of end effects and possible eccentricity of the wire. However, no observations were made concerning these effects.

Analysis of the Radioactive Xenon Sample

Characterizing and calibrating the detector were accomplished as described in the previous section. As a result, the effective analysis of the radioactive xenon sample should have been easily accomplished. However, for various reasons the 50-atmosphere analysis of the internal gas radioactive sample did not demonstrate the feasibility or utility of the detector for this purpose. Time to repeat this analysis was not available. Observations regarding the specifics of this analysis are presented in the subsections below.

Calibration. The energy calibration equation (6.7) presented in the previous section of these results also applies for the analysis of the internal gas sample.

Multiplication Factor. The detector was operated at a fill gas pressure of 50 atmospheres. However, as a result of limited purification processing, the detector could not be effectively operated above 2500 volts (cathode bias). The multiplication factor was determined at these conditions using the ^{241}Am source, prior to introducing the internal gas source. This multiplication factor was approximately 16.5.

Intrinsic Efficiency. Intrinsic efficiencies were also measured prior to the introduction of the internal gas source. The intrinsic efficiencies for ^{241}Am, ^{109}Cd and ^{57}Co were 2.78%, 2.54% and 3.56%, respectively. These efficiencies correlate well with those obtained during other 50-atmosphere data runs.

The intrinsic efficiency associated with the radioactive xenon gas source had to be approximated. A xenon gas sample (approximately 0.15 μCi) was obtained on 21 December 1983 by bleeding off a small amount of the radioactive gas from a larger 0.6 mCi gas source. The results of the analysis of the larger source, measured with a different calibrated detection system, were used to estimate (proportionately) the activities of ^{131m}Xe and ^{133}Xe in the smaller sample. Those results are listed below for the date of the analysis (29 December 1983):

$$\text{Activity } ^{131m}Xe \approx 5.15 \times 10^{-4} \text{ μCi}$$

$$\text{Activity } ^{133}Xe \approx 5.209 \times 10^{-2} \text{ μCi}$$

$$\text{Total Xe Activity} \approx 5.26 \times 10^{-2} \text{ μCi}$$

The ratio of ^{131m}Xe to ^{133}Xe was 1: 100 (as of the date of the analysis), and did not reach the desired 1: 50 ratio until on or about 10 January 1984.

As an internal sample, the geometric factor (fg) and the reduction factor for intervening materials (f_{ab}) were both one (100%). The fraction of electrons ($\beta^-_{avg} \approx 100.6$ keV) stopped in the detector, as calculated in Appendix B, was 93%. The branching ratio was taken considering the ^{133}Xe β^-'s only (0.993). The measured counts per counting time averaged 15.5 counts per second. The theoretical count rate in

the detector (^{133}Xe β^-'s only) was approximately 1739 counts per second. The efficiency was roughly 1%. This poor result can be immediately correlated to the one-thousand-fold increase in the experimental count rate, over count rates previously measured.

Resolution. The xenon signal resolution is approximated from those obtained for this fill gas run (prior to admixing the radioactive gas sample with the counting gas). The resolutions obtained at 2500 volts (cathode bias) were 6.1%, 8.3% and 11.0% for ^{241}Am, ^{109}Cd and ^{57}Co. Note that the slope of the associated log-log (resolution to energy) curve would have an improper positive slope. However, these data points suggest roughly a 10 keV (fwhm) for the 100.6 keV ^{133}Xe β^-_{avg}.

However, as a result of the reduced efficiency (~1%), low ^{131m}Xe concentration (~1%) and the probable 10^{-3} second required detector recovery time (missing 50%+ of all counts), the 164 keV conversion electron and x-ray/ Auger electron sum peak was not observed. Further complications were associated with high concentrations of impurities. The xenon sample (~10cc) underwent only one pass through the purification train, as contrasted to the twelve passes which the argon counting gas underwent.

Typical Spectra

Typical pulse height spectra which are representative of the fifty atmosphere results are presented in Figures 6.5 through Figures 6.8. The first three spectra were obtained with the external gamma ray sources (^{241}Am, ^{109}Cd and ^{57}Co). The last spectrum was obtained from the internal radioactive xenon gas test sample.

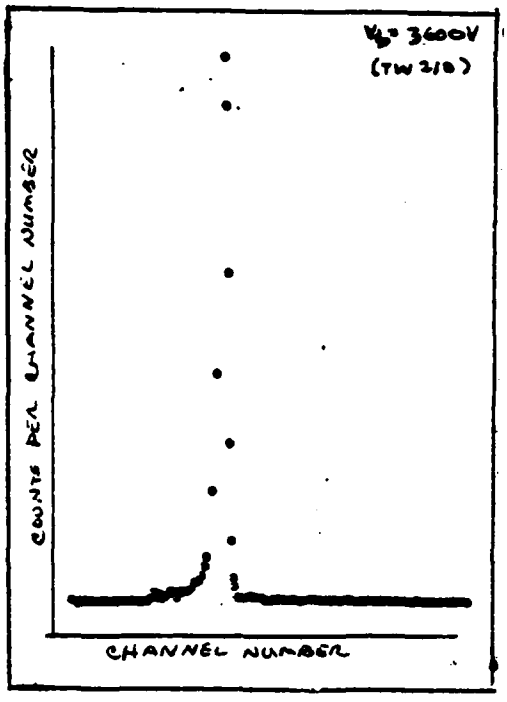

Figure 6.5. ^{241}Am
Experimental Spectrum

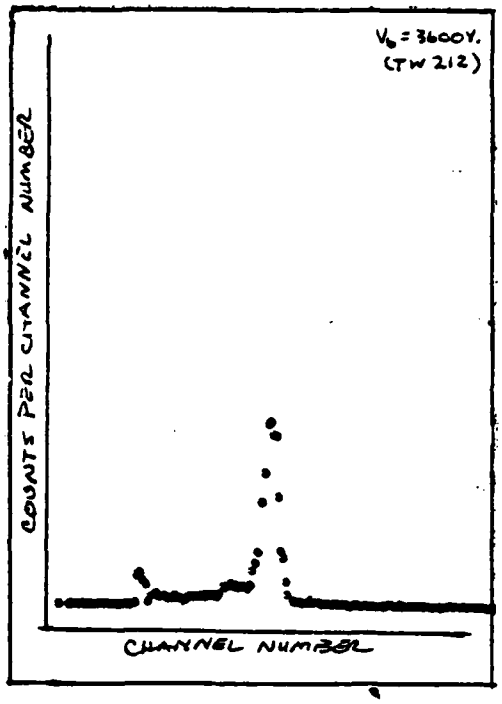

Figure 6.6. ^{109}Cd
Experimental Spectrum

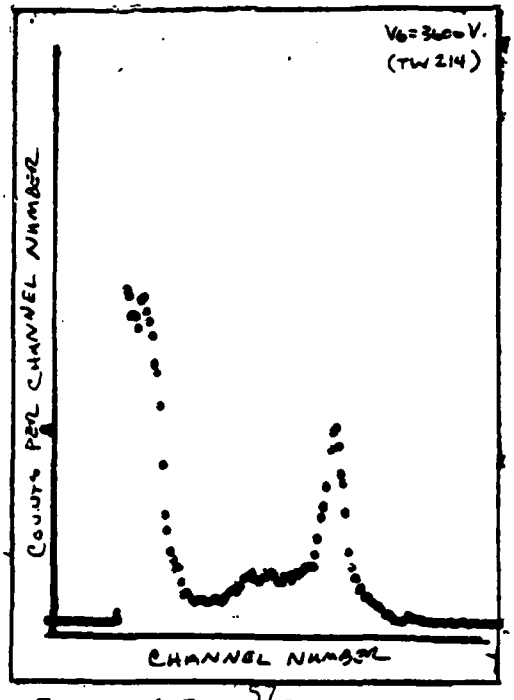

Figure 6.7. ^{57}Co
Experimental Spectrum

Figure 6.8. ^{131m}Xe & ^{133}Xe
Experimental Spectrum

VII. Conclusions and Recommendations

The conclusions drawn from this study suggest that the detector's response is effectively characterized to include energy calibration where voltages, gains and fill gas pressures are specified. However, the demonstration analysis of the radioactive xenon gas sample was unsuccessful due to excessively high ^{133}Xe activity and excessively low concentrations of ^{131m}Xe. The system is somewhat limited by the lack of a method to directly measure the detector pressure and is severely constrained by the use of an antiquated manual cryogenic purification process. A final problem area involves contaminants which apparently remain in the plexiglass insulators and epoxy seals of the end caps. Recommendations include replacing contaminated materials, recalibrating the detector and establishing an effective operational system through specific corrections to the limitations described.

Conclusions

The detector system's response is reasonably well characterized using the external gamma sources and energies investigated. The internal noble gas radionuclide was not successfully analyzed. However, minor changes to activities and concentrations used for test samples should allow future analysis with this system. System limitations regarding gas purification and gas pressure measurements currently reduce the utility of this system.

Calibration Relationships. The multiplication factors and the energy calibration relations are explicitly given in equation (6.6) and equation (6.7) for argon fill gas at 50 atmospheres of pressure.

The former is a function of voltage alone, while the latter is a function of voltage and gain settings. Errors of approximately 3% were found using these equations.

Intrinsic Efficiencies. Intrinsic efficiencies varied from 3.0-3.2% for 60-122 keV external gamma sources. Electron stopping efficiencies varied from 85-93% for 346-100.6 keV internal source betas.

Resolutions. Signal resolutions are approximately three times the limiting resolutions predicted by theory (eg ^{109}Cd $R_{TH} \simeq 3.33\%$, $R_{EXP} \simeq 8.8\%$). Resolutions were found to be best at 3400 volts cathode bias for 50-atmosphere argon fill gas. Resolutions at these operating conditions range from 7.5 to 9.1% for 60-122 keV photopeaks.

Noble Gas Source. The radioactive xenon internal gas source analysis was not successful. The ^{133}Xe activity was one hundred times the activity of the external sources used to calibrate the detection system. A total activity of 0.5 nCi should be ideal, whereas 0.5 μCi was the total activity of the actual test sample. This excessive source activity adversely affected the detector's electric field through space charge and general charge densities. Additionally, this excessive activity reduced the intrinsic efficiency to approximately 1.0%, as a result of counts missed during the detector's recovery time. Secondly, the concentration of ^{131m}Xe to ^{133}Xe was approximately 1: 100, rather than the planned 1: 50 ratio. The 164 keV ^{131m}Xe conversion electron-Xray / Auger electron sum peak was not observed, though a ^{133}Xe beta spectrum was observed.

Contamination. The detector's epoxy and plexiglass end cap insulators and seals are apparently contaminated and should be replaced before continuing work with this detector.

System Limitations. System limitations vary from inconveniences to severe deficiencies. The most challenging limitation is associated with the system's manual cryogenic purification system. Up to twelve hours of purification is required immediately prior to using the detector. Also, the required 1000°C operating temperature for the titanium and zirconium purification material (inside the quartz purification tube) is close to the quartz stress point. Continued use at these high temperatures frequently causes the tube to collapse when operated under a vacuum. Further, after initial purification of the gas, impurities develop from leaks and outgassing which reduce the detector's effectiveness in 3-5 days.

Detector Pressure Measurements. Though vacuum sealing is extremely effective ($\sim 10^{-7}$-10^{-8} torr), the reverse is not necessarily true. System leak rates at high pressures have not been adequately defined. Since pressures are not directly measured in the detector, multiplication factors may potentially vary a great deal as a consequence.

Recommendations

The essence of the recommendations regarding this system is to replace the contaminated end cap materials, to install automatic self-regulating purification systems and to resolve the pressure measurement problem. Once accomplished, it is recommended that the detector be recalibrated and have its operational capabilities verified with a second radioactive xenon gas sample analysis.

Purification Train. The purification system can be dramatically enhanced in four ways. The pre-use twelve-hour purification process can be automated by moving the current purification train to a position

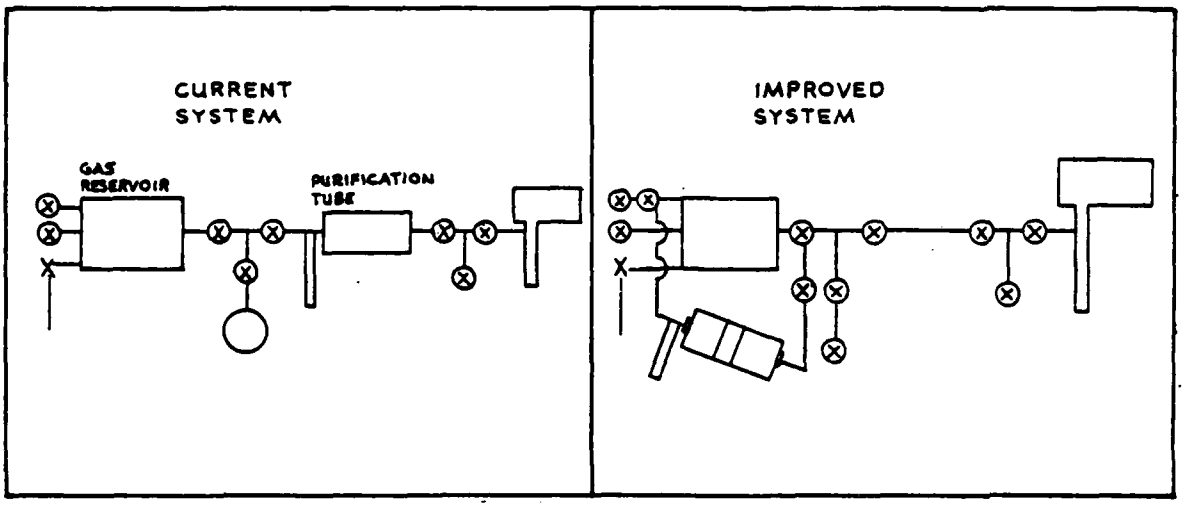

Figure 7.1. Improvement to Gas Purification System

directly underneath the gas reservoir as depicted in Figure 7.1.

The second improvement to the purification system would be to replace the Zr-Ti turnings operated at 1000°C with calcium turnings (outgas 750°C, operation 650°C) or 90% Ca-10% Mg mixtures (outgas 575°C, operation 475°C), as recommended by Gibbs et al (22:289). This would lower the operational temperature more than 250°C below the stress point of the quartz tubing with minimal effect on the purification process.

Third, install a small stainless steel high pressure purification chamber (typically 5-10% of the detector volume ~ 10-22 cc) to continuously purify the counting gas during the detector's operation. See Figure 7.2.

The last improvement to the purification system would be to investigate and develop a method to directly measure impurities. Current methods are essentially qualitative determinations.

Accurate Pressure Measurements. A direct measurement pressure

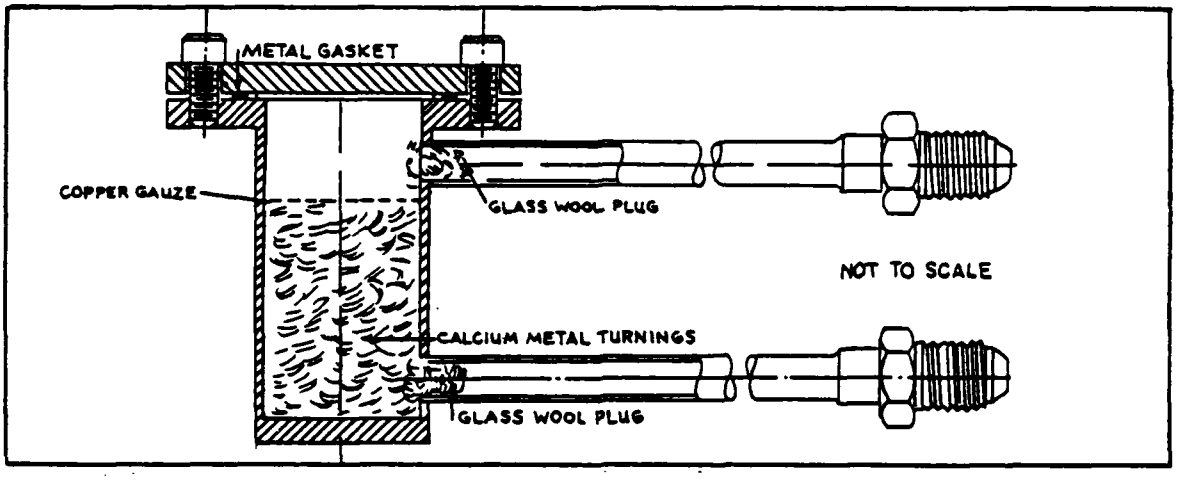

Figure 7.2. Continuous High Pressure Detector Purification System

gauge should be installed to allow accurate detector pressure readings. Such a gauge would allow pressure loss rates to be closely monitored. A control knob may be desired to isolate the gauge as required.

Future Detector Use. After replacing the end cap materials, installing the new purification systems (and materials) and after installing the direct pressure read-out gauges, I recommend that the detector be recalibrated. This should allow the successful analysis of a second radioactive xenon gas sample.

Bibliography

1. Andrews, Wayne L. Evaluation of a Detection System Employing Two Semiconductors for the Analysis of Radioactive Noble Gases. Unpublished thesis. Wright Patterson Air Force Base, Ohio: Air Force Institute of Technology, March 1982.

2. Baerg, A. P. "Pressurized Proportional Counters for Coincidence Measurements," Nuclear Instruments and Methods, 112: 95-99 (1973).

3. Bamberger, A. "High Pressure Proportional Counters Operating in Pure Hydrogen," Nuclear Instruments and Methods, 156: 107-110 (1978).

4. Bambynek, W. "On Selected Problems in the Field of Proportional Counters," Nuclear Instruments & Methods, 112: 103-110 (1973).

5. Batchelor, R. et al. "Helium-3 Filled Proportional Counter for Neutron Spectroscopy," The Review of Scientific Instruments, 26: 1037-1047 (November 1955).

6. Beneddeti, Dale. A Cryogenic Xenon Ionization Chamber Detector for Analysis of Radioactive Noble Gases. Unpublished thesis. Wright Patterson Air Force Base, Ohio: Air Force Institute of Technology, March 1983.

7. Bennett, W. R., Jr. "Glass Circulating Pump for Obtaining Noble Gases of High Purity," The Review of Scientific Instruments, 28: 1092-1093 (1957).

8. Berggren, Stephen R. A Cryogenic Argon Ionization Chamber Detector for Analysis of Radioactive Noble Gases. Unpublished thesis. Wright Patterson Air Force Base, Ohio: Air Force Institute of Technology, March 1982.

9. Bowe, J. C. "Drift Velocity of Electrons in Nitrogen, Helium, Neon, Argon, Kryton, and Xenon," Physical Review, 117: 1411-1415 (March 1960).

10. Campion, P. J. "A Study of Proportional Counter Mechanisms," International Journal of Applied Radiation and Isotopes, 19: 219-234 (1968).

11. Charles, M. W. "Gas Gain Measurements in Proportional Counters," Journal of Physics E: Scientific Instruments, 5: 95-100 (1972).

12. Charles, M. W. and R. Gott. "Attenuation of Proportional Counter Pulses by Equal Integrating and Differentiating Time Constants," Nuclear Instruments and Methods, 72: 157-160 (1969).

13. Chitwood, R. B. "Production of Noble Gases by Nuclear Fission," page 76 in Proceedings of the Noble Gas Symposium, ERDA CONF-730915, Stanley, R. E. and Moghissi, A. A., Editors, 1974.

14. Cockroft, A. L. and S. C. Curran. "The Elimination of the End Effects in Counters," The Review of Scientific Instruments, 22: 37-42 (January 1951).

15. Cook, G. A. and A. C. Jenkins. "Gas Phase Properties," Argon, Helium, and The Rare Gases, Cook, G. A., (Ed.). 1: 173-250, John Wiley & Sons, New York, 1961.

16. Costa, E. et al. "High Pressure MWPC for Hard X-ray Astronomy," Nuclear Instruments and Methods, 156: 57-61 (1978).

17. Crosswhite, H. M. and G. H. Dieke. "Eliminating Impurities from Noble Gases," Journal of the Optical Society of America, 42: 433 (1952).

18. Dean, J. A. (Ed.) Lange's Handbook of Chemistry, (12th Ed.) McGraw-Hill, New York, 1979.

19. Dodokhov, V. Kh. et al. "High Pressure Proportional Counter at Low Temperatures," Instruments and Experimental Techniques, 21(5): 1225-1227 (1978).

20. Fano, V. "Ionization Yield of Radiations. II. The Fluctuations of the Number of Ions," Physical Review, 72: 26-29 (July 1947).

21. Gibbons, M. R. Evaluation of a Gridded Ionization Chamber for the Detection of Radioactive Noble Gases. Unpublished thesis. Wright Patterson Air Force Base, Ohio: Air Force Institute of Technology, March 1984.

22. Gibbs, D. S. et al. "Purification of the Rare Gases," Industrial and Engineering Chemistry, 48: 289-296 (1956).

23. Gilmer, T. E. et al. "High Pressure Proportional Counter," The Review of Scientific Instruments, 28: 634-635 (August, 1957).

24. Groves, J. J. and G. R. Ricker. "Pulse Rise-times in Proportional Counters," Review of Scientific Instruments, 40: 227-233 (February 1969).

25. Gruhn, C. R. and R. Loveman. "A Review of the Physical Properties of Liquid Ionization Chamber Media," IEEE Transactions on Nuclear Science, NS-26 (1): 110-119 (February 1979).

26. Hallett, A. C. H. "Liquid-and Solid-State Properties," Argon, Helium, and The Rare Gases, Cook, G. A., (Ed.). 1: 313-390, John Wiley & Sons, New York, 1961.

27. Hampel, Clifford A., Editor. The Encyclopedia of the Chemical Elements. New York: Rheinhold Book Corporation, 1968.

28. Horrocks, D. L. and M. H. Studier. "Determination of Radioactive Noble Gases with a Liquid Scintillator," Analytical Chemistry. 36: 2077-2079 (1964).

29. Hunt, K. K. Analysis of a Semiconductor Detection System for Measuring Radioactive Noble Gases. Unpublished thesis. Wright Patterson Air Force Base, Ohio: Air Force Institute of Technology, December 1976.

30. Jenkins, A. C. "Summary of Physical Properties," Argon, Helium, and The Rare Gases, Cook, G. A., (Ed.). 1: 391-394, John Wiley & Sons, New York, 1961.

31. John, G. Unpublished class notes on Proportional Counters, Nucleonics Laboratory (NE 6.50); Air Force Institute of Technology, Wright Patterson Air Force Base, Ohio, 1983.

32. John, G. and R. Hagee. Final Report to Advanced Research Projects Agency on Project No. VT/2414, 1974.

33. Kaplan, I. Nuclear Physics (2d Ed.). Addison-Wesley, Reading, Mass., 1979.

34. Knapp, J. J. Study of the Characteristics of High Pressure Proportional Counters for the Detection of Radioactive Noble Gases. Unpublished thesis. Wright Patterson Air Force Base, Ohio: Air Force Institute of Technology, March 1983.

35. Knoll, Glenn F. Radiation Detection and Measurement. New York: John Wiley & Sons, 1979.

36. Kocher, D. C. Radioactive Decay Data Tables, Technical Information Center, U. S. Department of Energy, 1981.

37. Korff, Sage A. Electron and Neutron Counters. New York: D. Van Nostrand Company, 1955.

38. Lederer, C. M., et al. Table of Isotopes (Seventh Edition). New York: John Wiley & Sons, 1978.

39. Legrand, J., et al. "High-Pressure 4πProportional Counter for Internal Conversion Electron Measurements (^{139}Ce, ^{109}Cd, ^{99m}Tc)," Nuclear Instruments and Methods, 112: 101-102 (1973).

40. McMaster, W. H., et al. Compilation of Xray Cross Sections. UCRL-50174 Sec. II, Rev. 1. Livermore: Lawrence Radiation Laboratory, University of California, 1969.

41. Meek, M. E. and B. F. Rider. "Compilation of Fission Product Yields," Vallecitos Nuclear Center, ORNL-TM-3515, August, 1971.

42. Nelson, E. C. "Inert Atmospheres in Metallurgy," Argon, Helium, and The Rare Gases, Cook, G. A., (Ed.). 2: 609-634, John Wiley & Sons, New York, 1961.

43. Pisarev, A. F., et al. "A New Particle Detector - The Crystal Filament Counter," Soviet Physics JETP, 36: 828-834 (May 1973).

44. Povinec, Pavel. "A Study of Proportional Counter Optimization for Long-Term Counting," Nuclear Instruments and Methods, 163: 363-368 (1979).

45. Planeix, J. M. and E. F. Westrum, Jr. "Nuclear Applications," Argon, Helium, and The Rare Gases, Cook, G. A., (Ed.). 2: 569-608, John Wiley & Sons, New York, 1961.

46. Rossi, B. "Behavior of Electrons and Ions in Gases," Physical Review, 74: 1083 (1948).

47. Rossi, B. and H. H. Staub. Ionization Chambers and Counters. New York: McGraw Hill Book Company, Inc., 1949.

48. Rowe, Charles E. Quantitative Analysis of Radioactive Noble Gases with a SiLi Detector. Unpublished thesis. Wright Patterson Air Force Base, Ohio: Air Force Institute of Technology, March 1974.

49. Schell, W. R. "An Internal Gas Proportional Counter for Measuring Low Level Environmental Radionuclides," Proceedings of the 155th meeting of the American Chemical Society. San Francisco, Ca., April 1968.

50. Shibamura, E., et al. "Drift Velocities of Electrons, Saturation Characteristics of Ionization and W-Values for Conversion Electrons in Liquid Argon, Liquid Argon-Gas Mixtures and Liquid Xenon," Nuclear Instruments and Methods, 131: 249-258 (1975).

51. Siegbahn, Kai. Alpha-, Beta-, and Gamma-Ray Spectroscopy. Volumes I and II. Amsterdam: North Holland Publishing Company, 1966.

52. Sipila, H. "Inert Gas Mixtures for Proportional Counters," Nuclear Instruments and Methods, 140: 389 (1977).

53. Sipila, H. "Energy Resolution of the Proportional Counter," Nuclear Instruments and Methods, 133: 251-252 (1976).

54. Smith, B. L. Inert Gases: Model Systems for Science, Taylor & Francis, Ltd., London, 1971.

55. Wilkinson, D. H. Ionization Chambers and Counters, Cambridge University Press, Cambridge, 1950.

Appendix A

Critical Volumes in the Gas Handling System

The volumes of each subsection of the gas handling were measured by expanding a known volume of gas (1058.28 cm^3 ± 0.20 cm^3) into the volume of interest. Initial and final pressures were measured with a Wallace and Tiernan pressure gauge (Model FA 145). The pressures measured initially in the known volume and subsequently in the combined volumes were used to calculate the critical volumes using van der Waals equation. Table A.1 lists the measured volumes for the specific subsections of the gas handling system. Reference is made to valves depicted in Figure 4.1.

Table A.1

Critical Volumes in the Detection System

Volumes Between Valve Numbers	Section or Subsection Name	Volume (cm^3)	Uncertainty (cm^3)
1 - 2 - 3	Gas Reservoir	12,340	± 9.0
3 - 4 - 5	Left - 'T'	4.79	± 0.45
5 - 6	Purification Train	161.8	± 0.80
6 - 7 - 8	Right - 'T'	8.63	± 0.36
8 +	Detector	197.0	± 0.70

Appendix B

Calculation of Intrinsic Efficiency

The intrinsic efficiencies were calculated for the various energies and quanta emitted. Total counts measured versus total theoretical emissions stopped or absorbed (during the counting time) in the detector's sensitive volume are calculated using equations (2.2) through (2.9). Sample cross sections and specific results for the various factors are calculated in the following sections.

Geometric Factor Calculated

The external gamma sources are placed directly over the source wells. Calculations are made by assuming the source is concentrated at a point centered at the top of the source well. That well is modeled in Figure 6.1. Equation (2.5) is used to calculate the geometric factor, as below

$$fg = 0.5\ (1 - d/(d^2 + r^2)^{0.5}) \qquad \text{(B.1)}$$

$$fg = 0.5\ (1.0 - 0.65\ /\ ((0.65)^2 + (3/32))^{0.5})$$

$$\approx 5.12 \times 10^{-3}$$

where

d = 0.65 inches
r = 0.5 (3/16) inches

Transmission Factor for Intervening Material

Total absorption cross sections are used to calculate the reduction factors for intervening material, where scatters are assumed to be lost to the detector. As discussed in Chapter VI, iron cross

sections were used to simplify the calculations using equation (2.6). The 0.035-inch base of the source well was assumed to be the only significant intervening material. The 0.65-inch air gap between the source and the base of the source well was ignored. A sample calculation is presented in equation (B.2) for 60 keV photons. Reference data and results for other photon energies is presented in Table B.1.

$$f_{t\ Fe}^{60\ keV} = \exp\left(-(\mu/\rho)_t^{Fe}\ \rho_{Fe}\ X\right) \qquad (B.2)$$

$$= \exp\left(-(1.174 * cm^2/gm)(7.86\ gm/cm^3)(0.089\ cm)\right)$$

$$\simeq 0.44$$

Table B.1

Fe Total Absorption Reduction Factors

E_γ [keV]	$(\mu/\rho)_t^{Fe}$ [cm^2/gm][a]	f_t [b]
60	1.174	0.44
88	~ 0.4941	0.708
122	~ 0.2896	0.817

[a] (40); [b] $x \simeq 0.089$ cm, $\rho_{Fe} \simeq 7.86\ gm/cm^3$

Reduction Factors to Compensate for Photon Escape

Equation (2.7) was used to calculate the fraction of photons absorbed in the detector's sensitive volume. The fraction of photons which enter the detector and escape are calculated first; the balance are absorbed. Photoelectric interactions and Compton scatters are the interactions of principal interest. Argon cross sections are used. Gas densities are obtained from the ratio of the gram atomic weight of argon to its molar volume calculated using van der Waal's equation

(P = 50 or 20 atmospheres, T = 300°K). For external sources the distance 'X' was taken as the full detector diameter. Sample calculations are given in equations (B.3) to (B.5) for 60 keV photons. Reference data and other results are listed at Table B.2.

$$fs_{\gamma\ 50\ atm}^{60\ keV}(\tau) = 1.0 - \exp\left(-(\mu/\rho)_{\tau}\ \rho_{Ar}\ X\right) \qquad (B.3)$$

$$= 1.0 - \exp\left(-(0.2625\ cm^2/gm)(0.0848\ gm/cm^3)(4.128\ cm)\right)$$

$$\simeq 0.088$$

$$fs_{\gamma\ 50\ atm}^{60\ keV}(\sigma_c) = 1.0 - \exp\left(-(\mu/\rho)_{c}\ \rho_{Ar}\ X\right) \qquad (B.4)$$

$$= 1.0 - \exp\left(-(0.1357\ cm^2/gm)(0.0848\ gm/cm^3)(4.128\ cm)\right)$$

$$\simeq 0.046$$

$$fs_{\gamma\ 50\ atm}^{60\ keV} = fs_{\gamma\ 50\ atm}^{60\ keV}(\tau) + \int s_{\gamma\ 50\ atm}^{60\ keV}(\sigma_c) \qquad (B.5)$$

$$= 0.088 + 0.046 \simeq 0.134$$

Table B.2

Reduction Factors Compensating for Photon Escapes

E_γ [keV]	$(\mu/p)_\tau$ [a] [cm^2/gm]	$(\mu/\rho)\sigma_c$ [a] [$cm^2 gm$]	fs_γ [b],[d] (20 ATM)	fs_γ [c],[d] (50 ATM)
60	0.2625	0.1357	0.054	0.134
88	0.8464	~ 0.130	0.029	0.074
122	0.3652	~ 0.122	0.022	0.055

[a] (40); [b] ρ_{Ar} (20 atm, 300°K) ≃ 0.0331 g/cm^3; [c] ρ_{Ar} (50 atm, 300°K) ≃ 0.0848 g/cm^3; [d] x ≃ 4.128 cm

Reduction Factor to Compensate for Charged Particle Escapes

The quanta which interact with the fill gas ultimately result in energetic electrons. Also, the internal sources emit energetic electrons. Most of these electrons are stopped in the sensitive volume of the detector. The balance escape the fill gas and are absorbed by the detector case material. The development in Chapter II, which results in equation (2.9), allows this fractional loss to be calculated. A sample calculation for a 60 keV electron in argon at fifty atmospheres is given in equation (B.6) and (B.7). Other reference data and results are listed at Table B.3.

$$R^{60\ keV}_{e-\ 50\ atm}\ (cm) = R_{e-_{50\ atm}}\ (cm^2/g)\ /\rho_{A_r\text{-}50\ atm}\ (gm/cm^3) \qquad (B.6)$$

$$= (0.0090\ g/cm^2)\ /\ (0.0848\ g/cm^3)$$

$$\simeq 0.1061\ cm$$

$$f^{60\ keV}_{s_{e-}\ 50\ atm} = 0.75 + \frac{(b - R)^2\ (1 - 2R)}{4\ b^2\ l} \qquad (B.7)$$

$$= 0.75 + \frac{(2.064 - 0.1061)^2\ (6.223 - (2) \cdot (0.1061))}{4 \cdot (2.064) \cdot (6.223)}$$

$$\simeq 0.967$$

Table B.3

Reduction Factors Compensating for Charged Particle Escapes

E_{e-} [keV]	$R^{A_r}_{e-}$ [a] [g/cm^2]	$R^{A_r}_{e-}$ [b] (20 ATM)[cm]	$R^{A_r}_{e-}$ [c] (50 ATM)[cm]	$f_{s_{e-}}$ [d] (20 ATM)	$f_{s_{e-}}$ [d] (50 ATM)
60	0.009	0.2719	0.1061	0.922	0.967
88	0.017	0.5135	0.2005	0.868	0.941
100.6	0.020	0.6042	0.2358	0.851	0.931
122	0.029	0.8761	0.3420	0.809	0.905
164	0.045	1.3595	0.5310	0.766	0.864
346	0.150	4.5318	1.7690	-	0.752

[a] NBS circular 577, p.15, 1958; [b] ρ_{A_r} (20 atm) $\simeq$ 0.0331 gm/cm^3; [c] ρ_{A_r} (50 atm) $\simeq$ 0.0848 gm/cm^3; [d] b $\simeq$ 2.064 cm, l $\simeq$ 6.223 cm

Actual Source Activities

The activities of the sources were specified from National Bureau of Standards (NBS) surveys or were measured using previously calibrated detectors. Table B.4 summarizes the current source activity for the particular photons or charged particles listed (as of the date listed).

Table B.4

Activities of Sources Used

Source	Reference Activity (μCi) (Date: d-m-y)	Half-life	Branching Ratio, f_i	Current Particle or Photon Activity (29-12-83) $f_i \cdot S$ (dps)
^{241}AM	11.83 (1-6-82)	432.2 y.	0.359	15.67×10^4
^{109}Cd	65.51 (7-11-83)	453 d.	0.0361	8.081×10^4
^{133}Xe (β^- avg)	~0.149176 (21-12-83)*	5.27 d.	0.993	$\sim 5.2086 \times 10^{-2}$
^{57}Co (122 keV γ)	11.18 (1-6-82)	270.9 d.	0.8559	9.070×10^4
^{57}Co (136 keV γ)	11.18 (1-6-82)	270.9 d.	0.1061	
^{131m}Xe (C_{e^-})	$\sim 8.24 \times 10^{-4}$ (21-12-83)	11.8 d.	0.98	$\sim 5.15 \times 10^{-4}$

* All Betas

Intrinsic Efficiencies Calculated

The intrinsic efficiencies are calculated from the ratio of the measured counts to the theoretical counts calculated. The latter value

is obtained by combining equations (2.2) and (2.3). A sample calculation for ^{241}Am (60 keV photon) in argon at fifty atmospheres is given in equation (B.8). Measured count rates, theoretical count rates and associated intrinsic efficiencies for all sources used are summarized at Table B.5 and B.6 for twenty and fifty atmospheres, respectively.

$$\xi_{i\ 50\ atm}^{60\ keV\text{-}\gamma} = \frac{\text{Counts Measured}}{f_g \cdot f_{ab} \cdot f_{s_\gamma} \cdot f_{e-} \cdot (f_i \cdot S \cdot tc)} \qquad (B.8)$$

$$= \frac{\text{Counts Measured / tc}}{f_g \cdot f_{ab} \cdot f_{s_\gamma} \cdot f_{e-} \cdot (f_i \cdot S)}$$

$$= \frac{(10.45)}{(5.12 \times 10^{-3})(0.44)(0.134)(0.967)(15.67 \times 10^{4})}$$

$$\simeq 22.85\%$$

Table B.5

Experimental Intrinsic Efficiencies (20 ATM)

Source	Particle or Photon	Measured Count Rate 20 ATM(cps)	Theoretical Count Rate 20 ATM(cps)	Intrinsic Efficiency 20 ATM
^{241}Am	γ(60 keV)	2.95	17.58	16.8%
^{109}Cd	γ(88 keV)	2.09	7.37	28.3%
^{133}Xe	β^-_{avg}(100.6 keV)	-	-	-
^{57}Co	γ's(122 & 136 keV combined)	3.71	6.75	54.9%
^{131m}Xe	C_{e-}(164 keV sum peak)	-	-	-

Table B.6

Experimental Intrinsic Efficiencies (50 ATM)

Source	Particle or Photon	Measured Count Rate 50 ATM(cps)	Theoretical Count Rate 50 ATM(cps)	Intrinsic Efficiency 50 ATM
^{241}Am	γ(60 keV)	10.45	45.7	22.9%
^{109}Cd	γ(88 keV)	6.12	18.78	30.0%
^{133}Xe	β^-_{avg}(100.6 keV)	15.48	1797*	~1.0%
^{57}Co	γ's(122 & 136 keV, combined)	12.29	18.88	65.1%
^{131m}Xe	C_{e-}(164 keV sum peak)	-	-	-

* ^{131m}Xe and ^{133}Xe counts combined.

Appendix C

Comparison of Spectra (20 and 50 ATM)

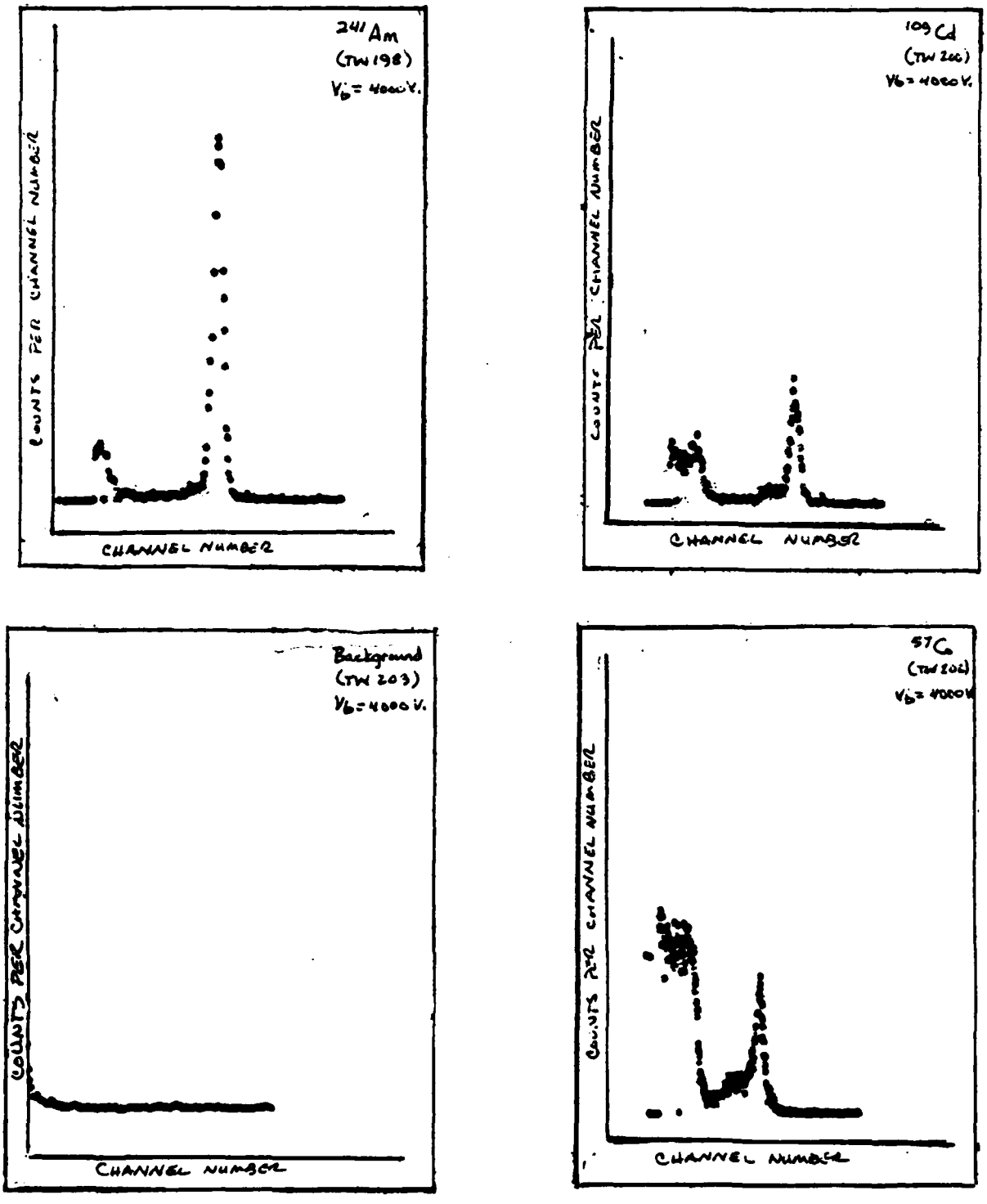

Figure C.1. Selected Spectra (20 ATM)

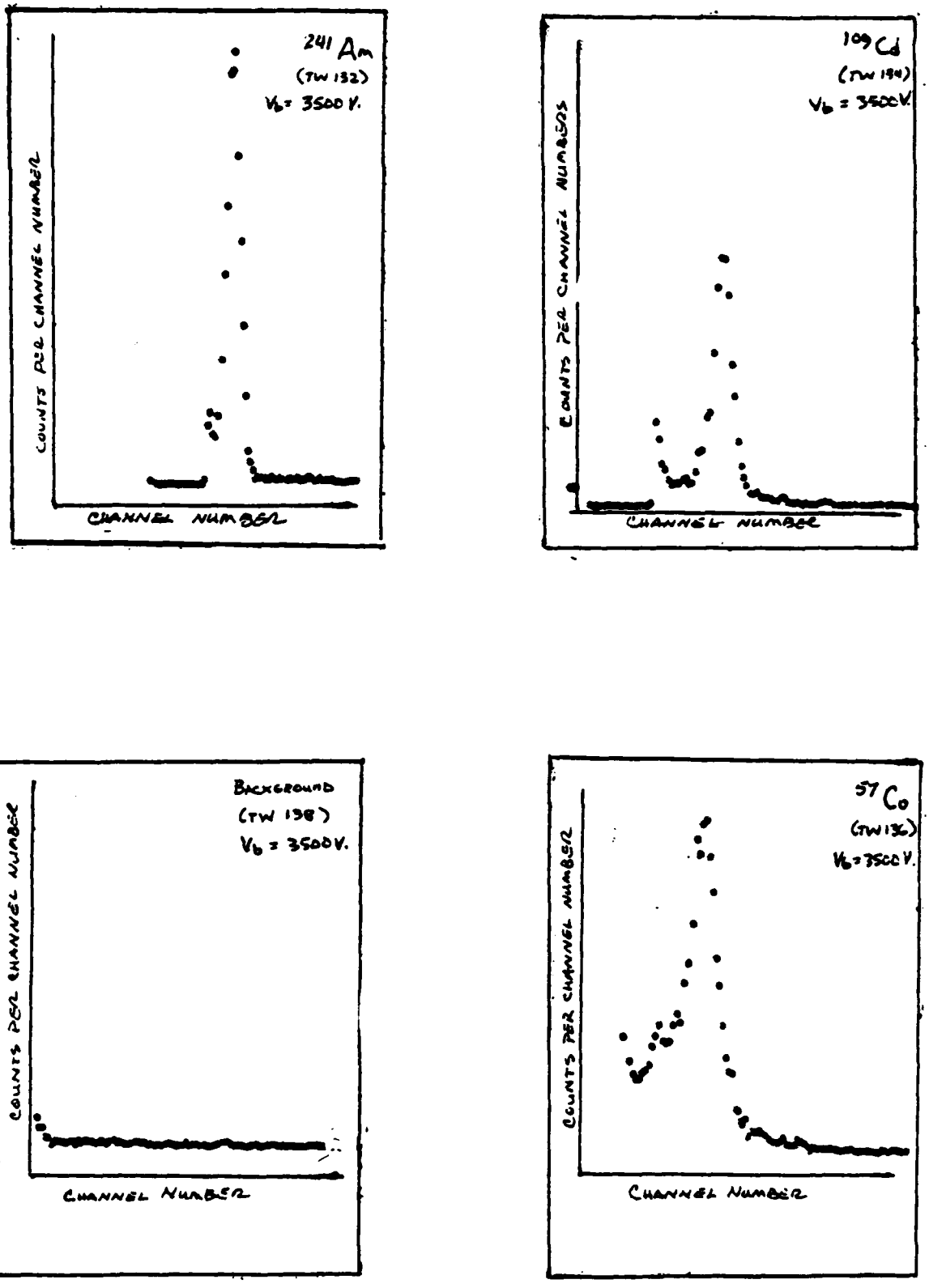

Figure C.2. Selected Spectra (50 ATM)

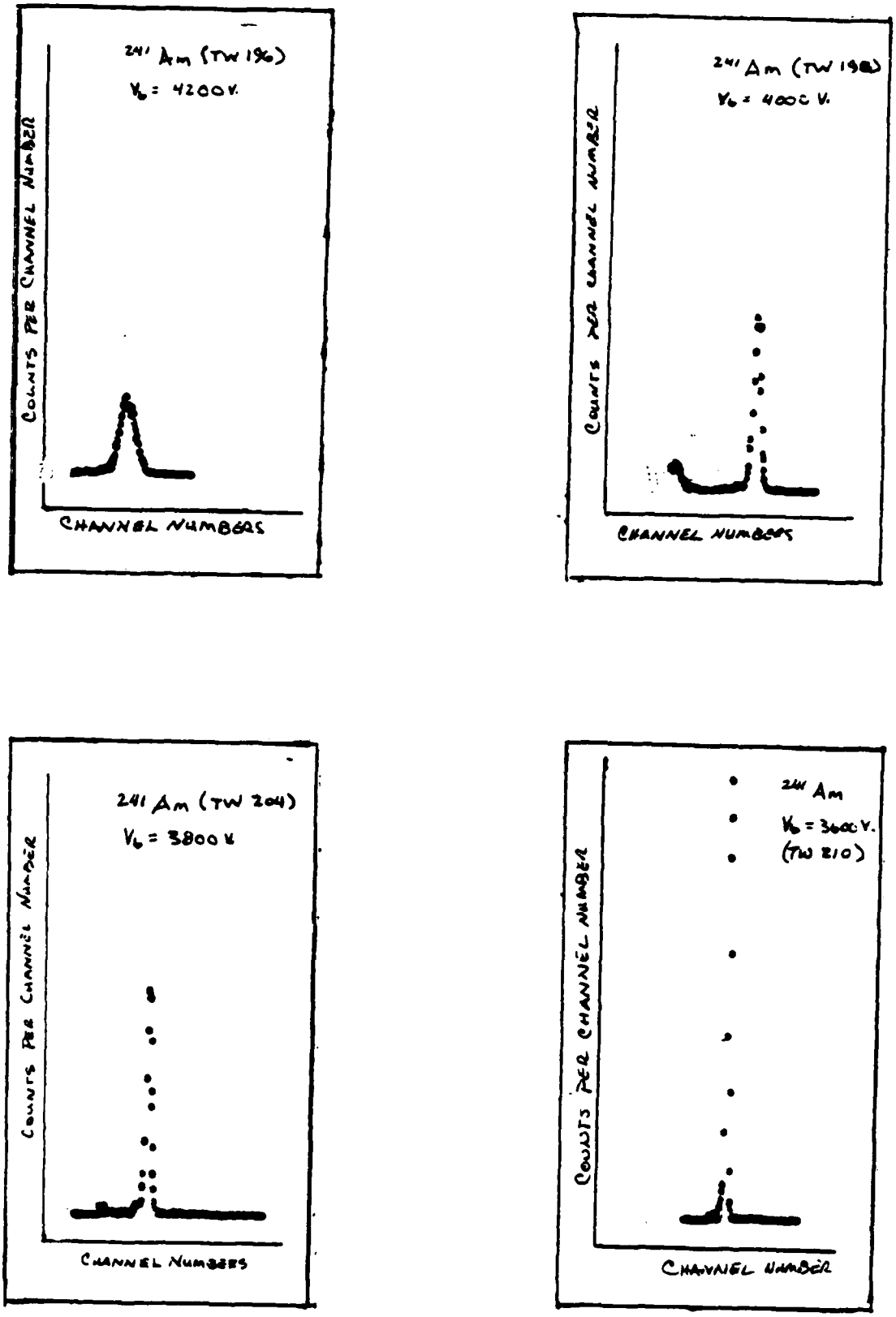

Figure C.3. Optimum Spectra (50 ATM)

Appendix D

Glossary of Symbols

Symbol	Meaning
a	anode radius
A	single electron multiplication factor
A_a	constant for Antoine vapor pressure equation
b	counter (cathode) radius
B	characteristic constant of the proportional counter (associated with the pulse shape curve)
B_a	constant for Antoine vapor pressure equation
C	capacitance of the proportional tube
C_a	constant for Antoine vapor pressure equation
C_i	concentration of impurities
C_{TH}	theoretical measured counts
d	distance of the detector from source
e	charge per electron
E_{dep}	energy deposited
f_{ab}	factor to account for losses of radiation quanta scattered or absorbed by source, air, windows or other intervening media
f_g	geometric factor which depends on source position, configuration and area of entrance window to detector
f_i	branching ratio of i-th quanta emitted
f_{max}	fraction of decays which do not deposit all of their energy in the detector
f_s	factor to account for quanta absorbed or stopped within the sensitive volume of the detector while the balance is considered to have escaped

$f_{s_{e-}}$	fraction of energetic electrons stopped in the detector's sensitive volume
f_{s_γ}	fraction of photons stopped within the sensitive volume
f_t	fraction of radiation transmitted through absorbers
fwhm	full width at half the maximum peak pulse height
" - ph	pulse height amplitude
" - det	limiting detector variance
" - noise	variance from circuit noise
" - i	other independent, additive and random effects
F	fano factor
K	minimum $\vec{\varepsilon}(r)/P$
l	counter length
M	multiplication factor
n_o	number of initial ion pairs
N_i	number of i-th quanta emitted
P	pressure [torr]
Q	total charge from all ion pairs
r	radius of circular detector surface
r_f	field tube radius
r_+	radial position of positive ion from anode wire
r_t	radius from anode where avalanche is initiated (threshold)
R	particle range
S	activity of the source
t	time from start of the multiplication process
ta	a characteristic time associated with the signal pulse shape curve of the counter
tc	counting time
T	temperature

V_+	average drift speed of the positive ions
$V_a(t)$	change in anode voltage across resistance in counter circuit (R_L in Figure 2.5)
Vb	voltage applied to the cathode
ΔV	Diethorn constant proportional to electric field associated with single electron ionizing events
V_f	field tube voltage
V_{max}	characteristic maximum voltage of the detector (defined Q/C)
W	average energy for the production of an ion pair
X	thickness of intervening material

Greek Symbols

α	first Townsend coefficient
β^-	beta particles
Δ	eccentricity of anode wire
$\delta\vec{\varepsilon}$	change in electric field
$\vec{\varepsilon}$	electric field
γ	gamma ray photons
λ	decay constant
μ	total absorption coefficient
$\mu+$	positive ion mobility
ρ	density
σ_c	Compton scatter coefficient
τ	photoelectric absorption coefficient

VITA

Richard Earl Lackey was born [redacted] Following graduation from high school [redacted] he entered the University of Maryland in September 1964. Drafted into the U.S. Army in 1967, he was commissioned via OCS as an Infantry officer in October 1968. Five years of subsequent Infantry assignments included a combat tour to the Republic of VietNam, two company level command assignments and two brigade level staff assignments. In 1973 he returned to the University of Maryland via the U.S. Army's degree completion program and earned the degree of Bachelor of Science in Chemical Engineering in May 1975. The following six years of Infantry assignments included an assignment to the recruiting command in Virginia, and four years in Europe which included a third company level command assignment, an assignment as Assistant Operations Officer for the 1st Armored Division, and an assignment as the Operations Officer for the 1st Battalion 51st Infantry. He subsequently graduated from the Command and General Staff College in June 1982 and entered the School of Engineering, Air Force Institute of Technology in August 1982.

Permanent address: [redacted]

UNCLASSIFIED
SECURITY CLASSIFICATION OF THIS PAGE

0129 816

REPORT DOCUMENTATION PAGE

1a. REPORT SECURITY CLASSIFICATION: UNCLASSIFIED	1b. RESTRICTIVE MARKINGS
2a. SECURITY CLASSIFICATION AUTHORITY	3. DISTRIBUTION/AVAILABILITY OF REPORT: Approved for public release; distribution unlimited.
2b. DECLASSIFICATION/DOWNGRADING SCHEDULE	
4. PERFORMING ORGANIZATION REPORT NUMBER(S): AFIT/GNE/PH/84M-9	5. MONITORING ORGANIZATION REPORT NUMBER(S)
6a. NAME OF PERFORMING ORGANIZATION: School of Engineering; 6b. OFFICE SYMBOL (If applicable): AFIT/ENG	7a. NAME OF MONITORING ORGANIZATION
6c. ADDRESS (City, State and ZIP Code): Air Force Institute of Technology, Wright-Patterson AFB, Ohio 45433	7b. ADDRESS (City, State and ZIP Code)
8a. NAME OF FUNDING/SPONSORING ORGANIZATION; 8b. OFFICE SYMBOL (If applicable)	9. PROCUREMENT INSTRUMENT IDENTIFICATION NUMBER
8c. ADDRESS (City, State and ZIP Code)	10. SOURCE OF FUNDING NOS. — PROGRAM ELEMENT NO. / PROJECT NO. / TASK NO. / WORK UNIT NO.
11. TITLE (Include Security Classification): See Box 19	
12. PERSONAL AUTHOR(S): Richard E. Lackey, B.S.Ch.E., MAJ, USA	
13a. TYPE OF REPORT: MS Thesis; 13b. TIME COVERED: FROM _____ TO _____; 14. DATE OF REPORT (Yr., Mo., Day): 1984 March; 15. PAGE COUNT: 130	
16. SUPPLEMENTARY NOTATION	

17. COSATI CODES		
FIELD	GROUP	SUB. GR.
18	04	
18	02	

18. SUBJECT TERMS (Continue on reverse if necessary and identify by block number): High Pressure Proportional Counter Detection System, Radioactive Noble Gases, Xenon

19. ABSTRACT (Continue on reverse if necessary and identify by block number)

Title: EVALUATION OF A HIGH PRESSURE PROPORTIONAL COUNTER FOR THE DETECTION OF RADIOACTIVE NOBLE GASES

Thesis Chairman: Dr. George John

Approved for public release: IAW AFR 190-17
LYNN E. WOLAVER 30 Apr 87
Dean for Research and Professional Development
Air Force Institute of Technology (AU)
Wright-Patterson AFB OH 45433

20. DISTRIBUTION/AVAILABILITY OF ABSTRACT: UNCLASSIFIED/UNLIMITED X SAME AS RPT ☐ DTIC USERS ☐	21. ABSTRACT SECURITY CLASSIFICATION: UNCLASSIFIED
22a. NAME OF RESPONSIBLE INDIVIDUAL: Dr. George John	22b. TELEPHONE NUMBER (Include Area Code): 513-255-5533; 22c. OFFICE SYMBOL: AFIT/ENP

DD FORM 1473, 83 APR — EDITION OF 1 JAN 73 IS OBSOLETE

UNCLASSIFIED
SECURITY CLASSIFICATION OF THIS PAGE

This report presents a study of the characteristics of a high pressure proportional detector for the qualitative and quantitative analysis of radioactive noble gases. Several external sources were used to establish the detector's response at high pressures (20 and 50 atmospheres) using argon fill gas. Radioactive xenon gas samples with Xe-131m and Xe-133 were used to test the detector. Aggressive gas purification techniques produced resolutions to 9% fwhm and intrinsic efficiencies of 3.2% or less. Unstable results were caused by contaminated end cap materials and electronegative impurities remaining after the manually performed purification process. Possible design changes for the detector are suggested.